ISSN: 0019-5693

INDIAN JOURNAL
OF
THEORETICAL PHYSICS

VOLUME 73 **NOS. 1, 2**

JANUARY, 2025 – JUNE, 2025

Published by the
CALCUTTA INSTITUTE OF THEORETICAL PHYSICS
(Formerly, INSTITUTE OF THEORETICAL PHYSICS)
"BIGNAN KUTIR"
4/1, MOHAN BAGAN LANE, KOLKATA-700004

(Peer-reviewed Journal)

ISSN: 0019-5693

INDIAN JOURNAL
OF
THEORETICAL PHYSICS

[Founder President: Late Prof. K. C. Kar, D. Sc.]

VOLUME 73 **NOS. 1, 2**

JANUARY, 2025 – JUNE, 2025

INDIAN JOURNAL
OF
THEORETICAL PHYSICS

"BIGNAN KUTIR"
4/1, MOHAN BAGAN LANE, KOLKATA-70004, INDIA

SUBSCRIPTION RATE

INDIA : For Library (Institute)

Rs. 1500.00 for each volume

FOREIGN : $ 350 for each volume

Drafts, Orders, Enquiries & Claim for Non-Receipt of Journal should be sent to:

CALCUTTA INSTITUTE OF THEORETICAL PHYSICS
(Formerly, INSTITUTE OF THEORETICAL PHYSICS)
"BIGNAN KUTIR"
4/1, MOHAN BAGAN LANE, KOLKATA-700004, India

C O N T E N T S

Elucidating the role of N-terminal Valine in determining the structural and binding properties of Hemoglobin: Computational approach

Madhurima Chakraborty [1], Nineesha Sen Banerjee[1, 2], and Tapan Ganguly[3]

[1]Department of Biochemistry, West Bengal State University, Kolkata- 700126, India

[2]Department of Biochemistry, Vivekananda College, Kolkata- 700063, India

[3] School of Laser Science and Engineering, Jadavpur University, Kolkata- 700032, India

[3] Email: tapcla@rediffmail.com

Abstract:

Human hemoglobin is a tetrameric protein and its functionality may depend on interactions involvingterminal amino acids. Moreover,hemoglobin is known to undergo non-enzymatic glycosylationin the free amino groupsby sugar moleculeslike glucose during hyperglycemia. Accordingly, we have studied the polar contacts of N-terminal Val1 in all four chains of HHb. Val1 of chain A and C appear to interact with ε-amino group of Lys127 possibly by hydrogen bonding interactions. The connections of Val1 with heme group of subunit B and C of HHb are also noted suggesting the role of Val1 in determining the overall structure of HHb during possible ligand binding.Furthermore, molecular docking studies of HHb with glucose also reveal involvement of Val1 and Lys99 of subunit A, heme group of subunit A and B along with other amino acid residues. Thus, our studyhighlights the possible contribution of Val1 within HHb and its glycated form. Also, the nature of involvement of Val1 in defining the structure, ligand binding and corresponding function is realized. This work may give insights regarding the mechanistic details of glycation andprovide novel insights in the field of clinical medicine, carbohydrate metabolism, protein chemistry and structural biology.

1 Introduction:

Hemoglobin is a protein found exclusively in red blood cells, giving the blood its bright red colour. Hemoglobin is an iron-containing metalloprotein whose key function is to carry oxygen from the lungs to all the cells in the body. It is comprised of two identical α-subunits (subunit A and C) and two identical β-subunits (subunit B and D)forming two identical dimers (A,B and C, D). The relative orientation of the dimers altersnotably in the ligand bound and non-bound state [1, 2].

Hemoglobin becomes glycated that is coated with glucose from the bloodstream if the blood glucose level rises. Along with increase in glucose level, more glucose binds to hemoglobin, developing a higher A1c value. The red blood cells have an average lifespan of about 90 days, and accordingly A1c test acts as an indicator tomonitor hemoglobin levels in the bloodstream within this time-frame. Thus, hemoglobin A1c also referred as glycated hemoglobin, glycosylated hemoglobin, HbA1c, or simply A1c—is used to assess sugar levels. The HbA1c test measures average blood sugar levels over the past 90 daysexpressed in percentage.Also, non-enzymatic glycation of proteins and lipids is triggered due to chronic hyperglycemia. This accelerates the damage caused in the small blood vessels of retina, kidney, and peripheral nerves, leading to complications such as diabetic retinopathy, nephropathy, and neuropathy [3-5].

The concept of the glycation of hemoglobin is illustrated by the following sequential stages as noted mostly from molecular docking studies using subunit B of hemoglobin. Firstly, reversible, noncovalent binding of glucose occurs at specific sitesof the protein. Secondly, reaction between the bound electrophilic glucose and nucleophilic amine residues of usually the N-terminal (α-amino) valine and internal (ε-amino) lysine residues to produce acovalently bound Schiff base or aldimine. Thirdly, rearrangement of the aldimine/Schiff

base to a Amadori intermediate takes place.Fourthly, the non-reversible formation of advanced glycation end products occurs[3-12]. Thus, the roles of various amino acid residues in differentstages of glycation becomes apparent. Moreover, glycation occurs in various sites to form different types of glycohemoglobin [3].

Here, we have investigated the polar contacts of N-terminal Val1 in determining the overall structure of HHb. Also, molecular docking analysis of entire HHb and glucose reveals the involvement of Val1, Lys residues and heme group. Overall, the study may suggest the role of Val1 in defining structure and function of HHb and highlightthe mechanistic details of glycation in hemoglobin which may have immense clinical and medicinal significance.

2.Materials and Methods:

The crystallographic coordinates of HHb, (PDB ID- 2DN2) is obtained from the Protein Data Bank (https://www.rcsb.org/) [13].

The binding of HHb with glucose is studied using the molecular docking server CB-Dock 2(https://cadd.labshare.cn/cb-dock2/php/index.php) [14]. CB-Dock2 server is used for protein-ligand blind docking, integrating cavity detection, docking and homologous template fitting. Here we have used the best docked model (minimum docking score) from structure based blind docking. When the three-dimensional structure of a protein and a ligand are uploaded, the server predicts the binding sites and affinity of docking.

For molecular docking, the x-ray crystal structure of HHb is obtained from RCSB PDB (PDB ID- 2DN2). The structure of ligand D-glucose is drawn using GaussView and optimized using Gaussian 09 program by DFT using the B3LYP method with basis set of LANL2DZ [15]. The docked complex having least amount of energy is visualized using PyMol (https://www.pymol.org/) [16].

3.Results and discussion:

Revealing the polar contacts of Val1 of each subunit of HHb

To understand the role of Val1 in determining the overall structure and binding of HHb, we plan to find out the polar contacts made by Val1 within HHb. The Val1 of each subunit of tetrameric HHb has been shown in **Figure 1**. **Figure 2** depicts the polar contacts of Val1 of the subunits of HHb.

For subunits A (**Figure 2A**), C=O group of Val1 is 2.9 Å away from ε-amino nitrogen of Lys127 of subunit A and on the other hand the same interacting atoms (C=O group of Val1) are 2.8 Å away from ε-amino nitrogen of Lys127 for subunit C(**Figure 2C**). Thus, Val1 and Lys127 are interacting with each other in subunit A and C.

Furthermore, since, HHb has two identical subunits (subunit A is identical to subunit C and subunit B is identical tosubunit D), thus,**Figure 2B** and **D**, clearly shows the similarity in bonding interactions of Val1 of subunits B and D both involving Leu3 and Leu78. Briefly, the C=O group of Val1 is 3.2Å from the NH group of Leu3 whereas NH of Val1 is 2.7 Å fromC=O group of Leu78 for subunit B (**Figure 2B**). Likewise, for subunit D(**Figure 2D**),the C=O group of Val1 is 3.9 Å fromthe NH group of Leu3 and the NH group of Val1 is 3 Å fromC=O group of Leu78.Thus, the amino acid residues surrounding Val1 (polar contacts of Val1) is observedfrom the above study.

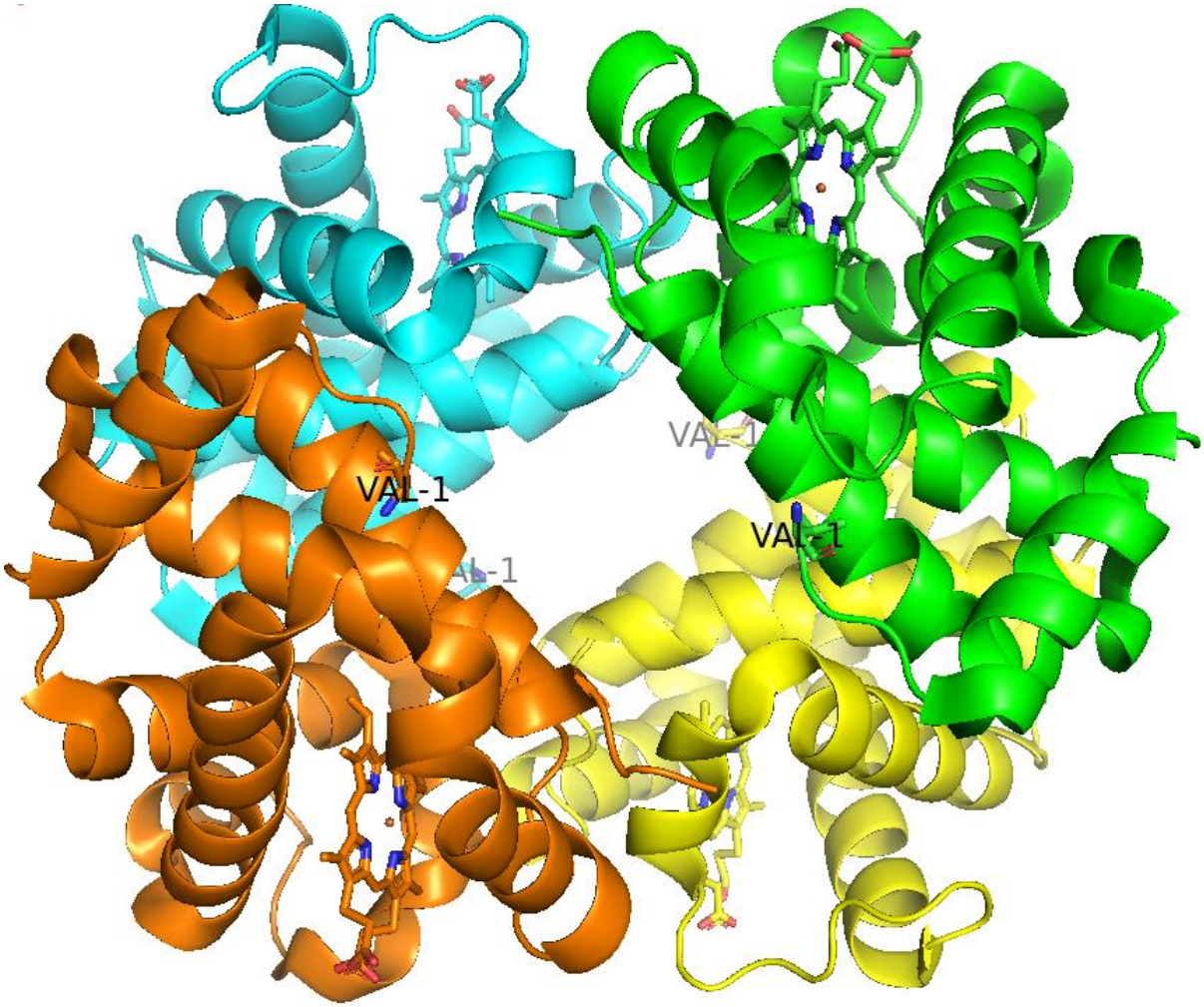

Figure 1: Representation of the tetrameric HHb with subunit A- cyan, subunit B- orange, subunit C- yellow and subunit D- green showing Val1 in stick mode in each of the subunits.

Role of Val1 in determining the overall structure of HHb through interactions with heme of the different subunits of HHb

Heme group is the probable binding site for known ligands of HHb like O_2 and the amino acids surrounding heme group may form the binding pocket for other small ligands of nano-dimension (nanoparticles, drugs, dyes, nutrients). Since, the heme group is buried in the folded polypeptide, thus, any ligand interacting with heme may affect the overall structure of HHb. Probably if Val1 has connections with the heme group of each subunit, either directly or indirectly then the role of Val1 in determining the overall structure of HHb can be

ascertained. Thus, we explore the connections of Val1 with the heme group, to understand its role in defining the overall structure of HHb.

Moreover, the interactions involving Val1 are stronger (lesser bond distances) for subunit B and C, thus we plan to check whether Val1 has any associationwith heme group of subunit B and C. Also, subunit B is identical to subunit D and subunit C is similar to subunit A and thus for simplicity consideringnon-identical subunits B and C seems logical.

For subunit B(**Figure 2B**), the methyl side chain of Leu78 (which is directly interacting with Val1) is 4 Å away from methyl side chain of Val133. The C=O group of Val133 is 2.8 Å distant from the NH group of Val137. The methyl group of Val137 is 4 Å away from the vinyl group of heme of subunit B.

In case of subunit C(**Figure 2C**), the C=O group of Lys127(which is directly interacting with Val1) is 3.5 Å far from the NH of Leu129. The C=O group of Leu129 is 3.4 Å distant from the NH group of Val132. The methyl group of Val132 is 4.2 Å away from the vinyl group of heme of subunit C.Thus, it seems that if any ligand interacts with Val1, then such interactions may affect the overall structure of HHb by altering microenvironment surrounding heme.

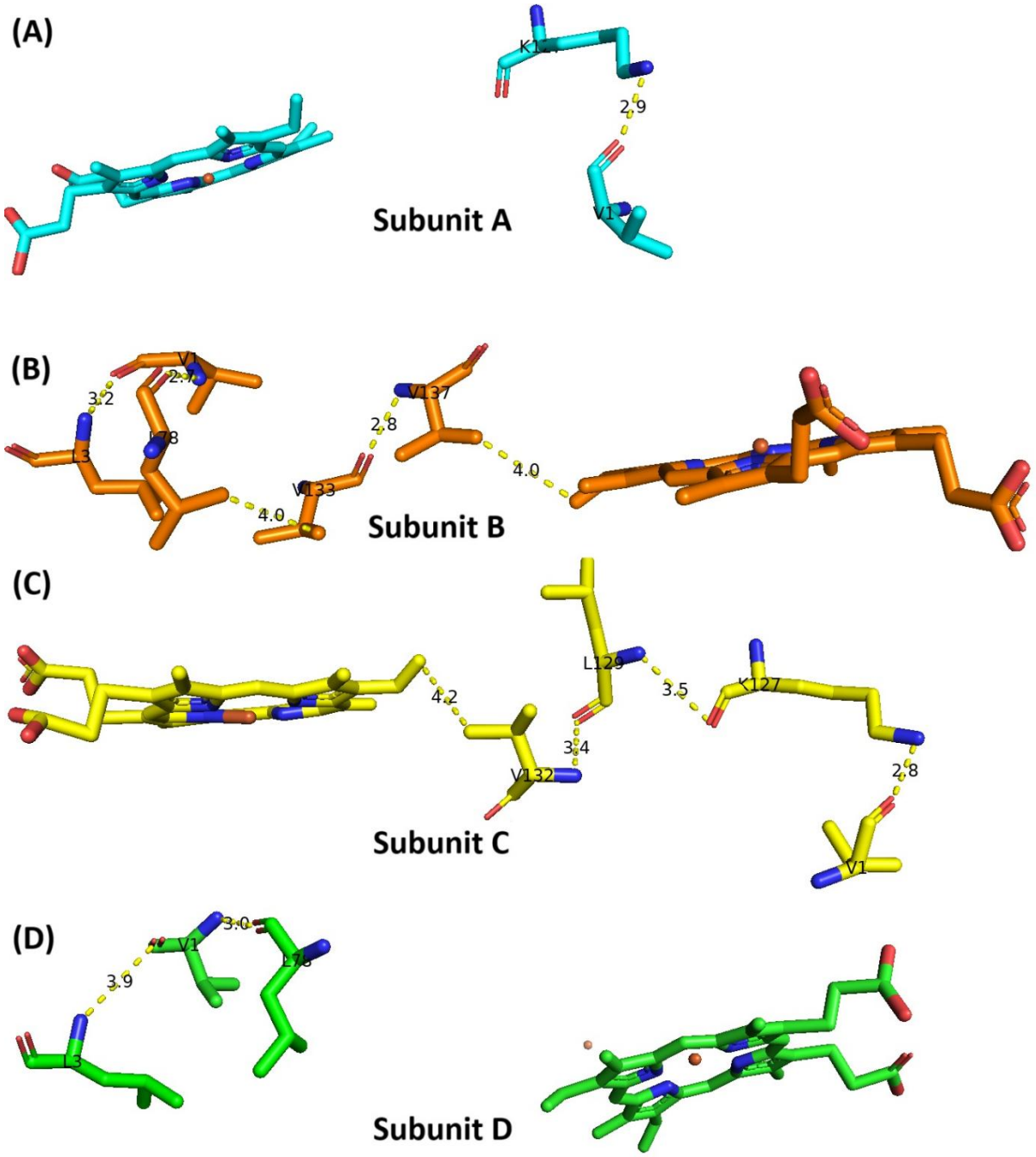

Figure 2:Representative images showingpolar contactsof Val1 for subunits A (**A**), subunit B (**B**), subunit C (**C**) and subunit D (**D**) has been displayed.Numbers indicate bond distances.

Secondary structural features of HHb and amino acid residues involved in polar contacts with Val1

As a next step, we plan to study the secondary structural features of the interacting residues involving Val1 of HHb. This may help to understand the alterations in secondary

structural characteristicsof HHb during interactions with ligands. **Figure 3A**indicates theα-helical formto be the predominant secondary structural type in HHb.

Additionally, assessment of the interacting residues shows that Val1, Leu3 and Leu78 to be part of loop in subunit B and D whereas Leu78 of subunit B and Lys 127 of subunit A and C are a part of α-helix(**Figure 3B**). Thus, alterations in both α-helical and coil forms may be expected if interactions involving Val1 of HHb occurs.

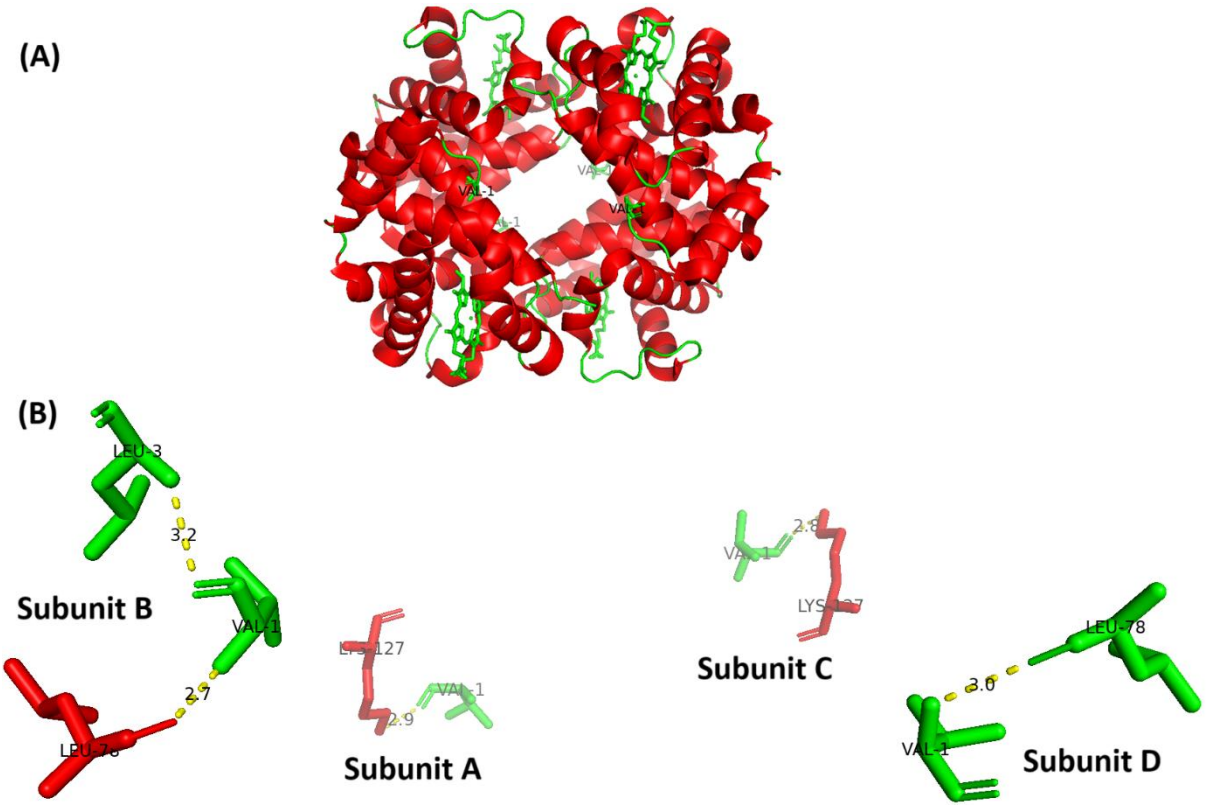

Figure 3: (**A**) Representative view of HHb showing its secondary structural features(α-helix-red and coil-green). Val1 is displayed in stick mode in each of the subunits. (**B**) Secondary structural features of amino acid residues involved in polar contacts of Val1.Numbers indicate bond distances.

Molecular docking analysisHHbwith glucose

As a next step, we plan to study the interaction of HHb and glucose by molecular docking analysis. The purpose is to check the role of Val1 and its surrounding residues involved in polar contacts along with heme group during interaction with glucose

molecule.Surface representation of the docked structure of HHb with glucose is represented in **Figure 4A**. The docking score forprediction of binding affinity appears to be -5.3. Here, the conformation with minimum docking score is taken as the best binding pose and the corresponding site is the optimal binding site for the query ligand.

The involvement of amino acid residues surrounding 4 Å of glucose molecule at the docked position within HHb has been discussed. The C1-OH of glucose is 2.6 Å away from the C=O of Lys99, 3.9 Å distant from the NH group of Leu100 and 4 Å far from the CH_2 group in side chain of His103 of subunit A. The C2-OH of glucose is 4 Å distant from the CH_2 group in side chain of Lys99 of subunit A and 3.9 Å away from the methyl side chain of Leu105 of subunit B. Interestingly, the C=O group of Asn102 is 3.4 Å from NH group of Leu105 and 3.6 Å from the methyl group of heme of subunit B. The C3-OH of glucose is 2.1 Å from OH group of Tyr35 of subunit B. The C4-OH of glucose is 2.9 Å away from the guanidium NH of Arg141 of subunit C. The C=O of this Arg141 of subunit C is 4.4 Å from the C=O group of Val1 of subunit A.The C6-OH is 3.9 Å the OH side chain of Ser102, 3.5 Å from NH group of Leu129 and 2.2 Å from NH group of Ala130 of subunit A.The methyl group of Leu129 and OH side chain of Ser102 is 5.1 Å and 5.2 Å away respectively from the vinyl group of heme of subunit A. Overall, the contacts involving glucose and the amino acid residues are mostly hydrogen bonding type.

Therefore, from the above interaction study,we can understand the role of Val1 of subunit A and the heme group of subunit A and Bduring interaction with glucose. The interactions may also affect the overall structure of HHb since amino acids and heme from different subunits are getting involved in interactions. All in all, the observations may support to highlight the mechanistic details of glycation in hemoglobin which may have wide-range of significance particularly in the fields of clinical diagnosis and medicine, cellular metabolism, structural biology protein chemistry and many more.

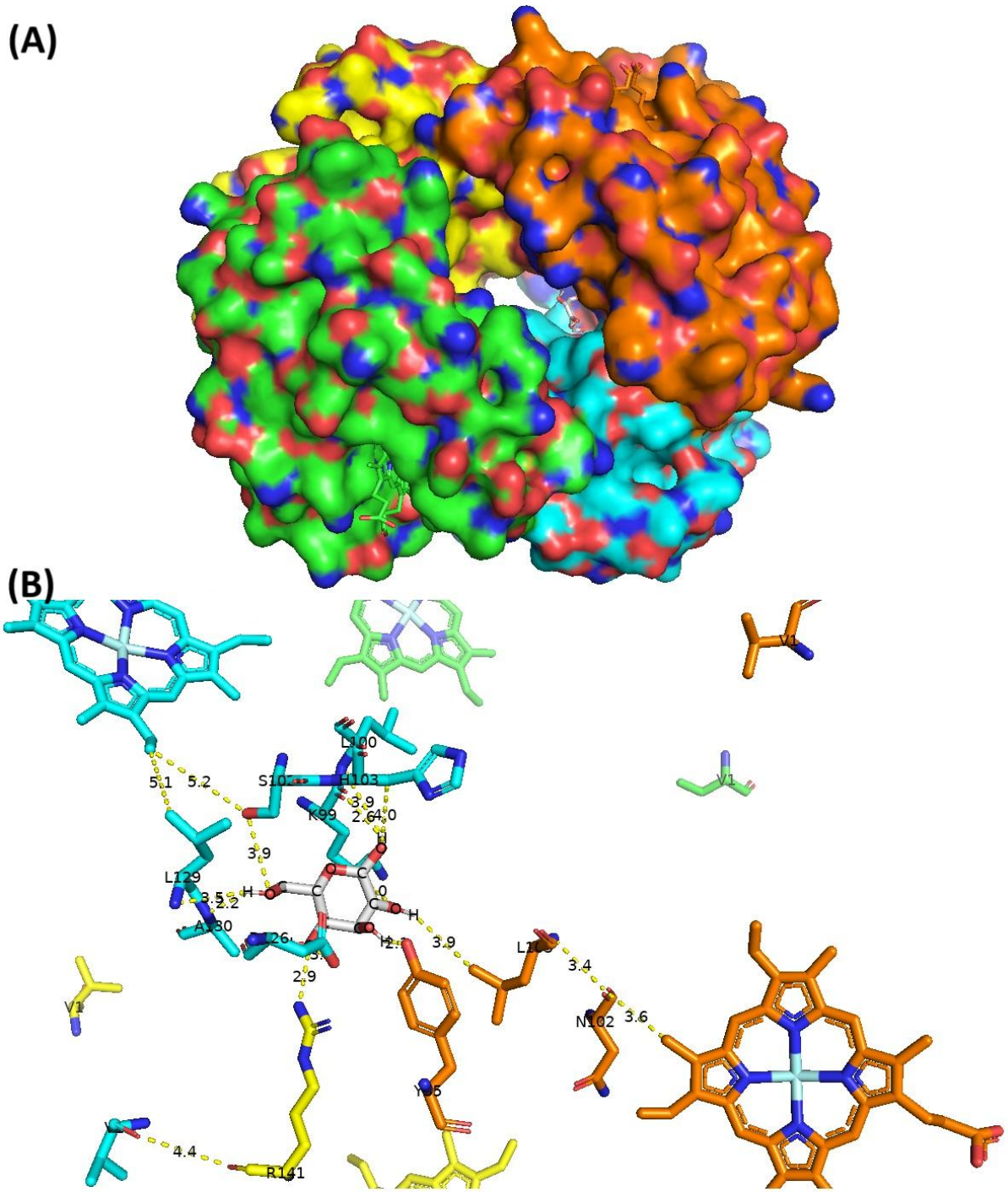

Figure 4: (a) Surface representation of the docked structure of HHb and glucose is shown, subunit A- cyan, subunit B- orange, subunit C- yellow and subunit D- green. (b) Interaction of amino acid residues surrounding 4 Å of docked glucose. Numbers indicate bond distances.

4.Conclusions

Assessment of polar contacts ofVal1 suggests its role in determining the overall structure of HHb. Also, the amino acids involved in polar contacts with Val1 further highlights the important role of Lys residues within HHb. Moreover, the possible sites of glycation in HHb as detected by molecular docking study of HHb and glucose also reveal the involvement of Val1 and heme group along with other amino acid residues. Overall, our study may give insights to understand the mechanistic details of glycation in hemoglobinandprovide fruitful insights in the field of clinical physiology, protein chemistry, structural biology, and others.

References

[1] El Hage, K., Hedin, F., Gupta, P. K., Meuwly, M., & Karplus, M. (2018). Valid molecular dynamics simulations of human hemoglobin require a surprisingly large box size. *Elife*, *7*, e35560.

[2] Baldwin, J., & Chothia, C. (1979). Haemoglobin: the structural changes related to ligand binding and its allosteric mechanism. *Journal of molecular biology*, *129*(2), 175-220.

[3] Weykamp, C., John, W. G., & Mosca, A. (2009). A review of the challenge in measuring hemoglobin A1c. *Journal of diabetes science and technology*, *3*(3), 439-445.

[4] Bunn, H. F., Haney, D. N., Kamin, S., Gabbay, K. H., & Gallop, P. M. (1976). The biosynthesis of human hemoglobin A1c. Slow glycosylation of hemoglobin in vivo. *The Journal of clinical investigation*, *57*(6), 1652-1659.

[5] Malka, R., Nathan, D. M., & Higgins, J. M. (2016). Mechanistic modeling of hemoglobin glycation and red blood cell kinetics enables personalized diabetes monitoring. *Science translational medicine*, *8*(359), 359ra130-359ra130.

[6] Eyth, E., & Naik, R. (2023). Hemoglobin A1C.[Updated 2023 Mar 13]. *StatPearls [Internet]. Treasure Island (FL): StatPearls Publishing; Jan. Available: https://www. ncbi. nlm. nih. gov/books/NBK549816*.

[7] WHO Guidelines Approved by the Guidelines Review Committee. (2011). Use of glycated haemoglobin (HbA1c) in the diagnosis of diabetes mellitus: abbreviated report of a WHO consultation. *Geneva: World Health Organization*, *3*.

[8] Clark, S. L., Santin, A. E., Bryant, P. A., Holman, R. W., & Rodnick, K. J. (2013). The initial noncovalent binding of glucose to human hemoglobin in nonenzymatic glycation. *Glycobiology*, *23*(11), 1250-1259.

[9] Holmquist, W. R., & Schroeder, W. A. (1966). A new N-terminal blocking group involving a Schiff base in hemoglobin AIc. *Biochemistry*, *5*(8), 2489-2503.

[10] Franklin Bunn, H. (1981). Evaluation of glycosylated hemoglobin in diabetic patients. *Diabetes*, *30*(7), 613-617.

[11] Makita, Z., Vlassara, H., Rayfield, E., Cartwright, K., Friedman, E., Rodby, R., ... & Bucala, R. (1992). Hemoglobin-AGE: a circulating marker of advanced glycosylation. *Science*, *258*(5082), 651-653.

[12] Koenig, R. J., Blobstein, S. H., & Cerami, A. N. T. H. O. N. Y. (1977). Structure of carbohydrate of hemoglobin AIc. *Journal of Biological Chemistry*, *252*(9), 2992-2997.

[13] Park, S. Y., Yokoyama, T., Shibayama, N., Shiro, Y., & Tame, J. R. (2006). 1.25 Å resolution crystal structures of human haemoglobin in the oxy, deoxy and carbonmonoxy forms. *Journal of molecular biology*, *360*(3), 690-701.

[14] Liu, Y., Yang, X., Gan, J., Chen, S., Xiao, Z. X., & Cao, Y. (2022). CB-Dock2: improved protein–ligand blind docking by integrating cavity detection, docking and homologous template fitting. *Nucleic acids research*, *50*(W1), W159-W164.

[15] Gaussian 09, Revision A.02, M. J. Frisch, G. W. Trucks, H. B. Schlegel, G. E. Scuseria, M. A. Robb, J. R. Cheeseman, G. Scalmani, V. Barone, G. A. Petersson, H. Nakatsuji, X. Li, M. Caricato, A. Marenich, J. Bloino, B. G. Janesko, R. Gomperts, B. Mennucci, H. P. Hratchian, J. V. Ortiz, A. F. Izmaylov, J. L. Sonnenberg, D. Williams-Young, F. Ding, F. Lipparini, F. Egidi, J. Goings, B. Peng, A. Petrone, T. Henderson, D. Ranasinghe, V. G. Zakrzewski, J. Gao, N. Rega, G. Zheng, W. Liang, M. Hada, M. Ehara, K. Toyota, R. Fukuda, J. Hasegawa, M. Ishida, T. Nakajima, Y. Honda, O. Kitao, H. Nakai, T. Vreven, K. Throssell, J. A. Montgomery, Jr., J. E. Peralta, F. Ogliaro, M. Bearpark, J. J. Heyd, E. Brothers, K. N. Kudin, V. N. Staroverov, T. Keith, R. Kobayashi, J. Normand, K. Raghavachari, A. Rendell, J. C. Burant, S. S. Iyengar, J. Tomasi, M. Cossi, J. M. Millam, M. Klene, C. Adamo, R. Cammi, J. W. Ochterski, R. L. Martin, K. Morokuma, O. Farkas, J. B. Foresman, and D. J. Fox, Gaussian, Inc., Wallingford CT, 2016.

[16] Li, X., Li, H., Lai, K., & Miao, J. (2023). The Effect of Glucose on the Interaction of Bisphenol A and Bovine Hemoglobin Characterized by Spectroscopic and Molecular Docking Techniques. *International Journal of Molecular Sciences*, *24*(19), 14708.

Pulsatile Non-Newtonian Blood Flow through a Narrow Stenosed Artery with slip at the Stenotic Wall

Dr Malay Sanyal[1] and Sayantani Ghosh[2]

1 Department of Mathematics, Ranaghat College, University of Kalyani, Ranaghat 741201, West Bengal, India

2 Department of Mathematics, Ranaghat College, University of Kalyani, Ranaghat 741201, West Bengal, India

*Corresponding author's E-mail(s): malaysanyal4@gmail.com; sayantanighosh18@gmail.com;

Abstract

This study investigates the pulsatile flow of non-Newtonian blood through a narrow artery with mild stenosis, considering the effects of periodic body acceleration and slip velocity at the stenosed vessel wall. The governing nonlinear partial differential equations are solved analytically using the perturbation method under appropriate boundary conditions. Expressions for the velocity profile, volumetric flow rate, and shear stress are derived and analyzed numerically. The results reveal that in the stenosed region, both velocity and volumetric flow rate decrease significantly due to plaque formation, which obstructs blood flow near the constricted wall. Additionally, retrograde motion of blood near the wall increases resistance to incoming flow. The study also highlights the significant influence of slip velocity and periodic body acceleration on blood flow dynamics in the stenotic region. These findings provide valuable insights into arterial blood flow behavior and may contribute to the understanding of cardiovascular diseases associated with arterial narrowing.

Keywords: non-Newtonian fluid, stenotic region, stenosis, body acceleration, pulsatile flow, slip velocity

1 Introduction

Blood vessels play a vital role in cardiovascular system. Arteries transport oxygen- rich blood ,along with red blood cells, white blood cells ,nutrients and other essential substances from the heart to various parts of the body. In contrast, veins carry blood with carbon dioxide and various devoid of substances back to heart. Arteries are strong flexible blood vessels capable of contracting and expanding with each heartbeat, whereas veins are less flexible. Flexibility of the artery is largely maintained by a thin layer of cells which known as the **endothelium**, which allows smooth and efficient blood flow. When the endothelium is damaged-due to factors -such as high blood pressure, high cholesterol or smoking then **Low Density Lipoprotein (LDL)** cholesterol tends to accumulate at the damaged site. The body responds by sending **macrophage white blood cells** to repair the damage, but these cells can also become trapped in the damaged area. As the process continue the **plaque** builds up, thickening arterial wall and narrowing the lumen through which blood flow. This process is known as **atherosclerosis**. As a result, the wall of the artery loses its elasticity and the blood flow to the corresponding organ become impaired. This abnormal narrowing of the artery is called **stenosis**[1- 6].

Over past decades both theoretical and experimental studies have been conducted on blood flow through stenosed artery. It is now well established that hydrodynamics factors such as resistance to the flow, wall shear stress and apparent viscosity have an important role in the formation and progression of arterial stenosis [5, 9, 11, 16 ,17]. Young [5] addressed several fundamental problems of blood flow through stenosed arteries. Verma et. al. [16] studied the effect of stenosis shape on arterial blood flow under conditions of mild stenosis.

Blood exhibits **anomalous viscous properties** because it is a suspension of cells in plasma. While plasma behaves as a Newtonian fluid, whole blood often displays **non-Newtonian properties**, especially at low shear rates, as observed in small arteries and downstream of stenosed regions. At high shear rates, such as in large arteries, blood behaves more like a Newtonian fluid[7]. Additionally, the **viscoelasticity** of blood decreases significantly with increasing shear rate in arteries of larger diameter.

Pries et al [15] studied the effect of tube diameter and **hematocrit ratio** on blood viscosity . They concluded that the tube diameters greater than 1 mm, the blood viscosity is relatively unaffected by diameter while for diameter less than 1 mm, viscosity increases non-linearly with hematocrit. Furthermore, blood velocity is strongly depended on tube diameter in smaller vessels.

The cyclic nature of heart pumping leads to **pulsatile condition**s in blood flow. Rabby et al [27]suggested that during pulsatile motion, blood flow tends to have a low Reynold's number ,especially during diastole, early systole and within stenosed regions. In these cases, the **non-Newtonian behavio**r of blood becomes particularly relevant. Chien [6] found that non-Newtonian properties are more prominent under pathological conditions such as **cerebrovascular disease, myocardial infarction and hypertension.**

In everyday life, the bodies often subjected to **periodic acceleration** during activities such as sports , high speed travel, or flying. Arntzenius et al[3] demonstrated that external disturbance on the body has significant effect on blood circulation. Consequently, it is important to consider **periodic body acceleration** in studies of pulsatile blood flow. Sud and Sekhon [10] developed a mathematical model of blood flow in arteries under pulsatile pressure gradient and body accelerations. Chaturani and Palanisamy [13] extended this work by studing the pulsatile flow through rigid tubes under similar conditions and later incorporated non- Newtonian characteristics into their model [14] .

Another important factor in stenosed arteries is the slip velocity at the vessel wall. Sanyal[28] considered pulsatile flow through elastic tube with wall slip. Misra and Shit [17] developed mathematical model of blood flow through stenosed artery considering wall slip at the constricted region. More rrecently Ponalagusamy[21]and Biswas and Chakraborty[25] examined blood flow through stenosed arterial segment with wall slip treating blood as a Newtonian fluid.

The motivation of the paper is to investigate the unsteady pulsatile flow of non -Newtonian blood through an arterial segment with **time-dependent stenosis**, incorporating the effect of **periodic body acceleration** and **slip velocity at the constricted wall**. Unlike some previous models, this study considers blood as a **non-Newtonian fluid** to better capture realistic physiological conditions.

We formulated the problem mathematically, non-dimensionalize the governing equations and boundary conditions, and solve The resulting non-linear differential equations using by perturbation method. Analytical expression for the **velocity, flow rate, wall shear stress, effective viscosity** are obtained. These expressions are evaluated numerically and analyzed graphically under specific condition to clearly illustrate how this flow parameters vary with different physical and physiological factors.

2 Mathematical Formulation

Consider a pulsatile axially symmetric one-dimensional and fully developed flow of blood (assumed to be incompressible and non-Newtonian) in a narrow artery with stenosis. The geometry of the stenosis in artery is shown in **Figure. 1.** The cylindrical polar co-ordinate ($\bar{r}$, $\bar{t}$, $\bar{z}$) is introduced to analyze the flow. Since the artery is narrow, we neglect the radial velocity.

Arterial stenosis given by the mathematical model [22]

$$\bar{R}(\bar{z}) = \bar{R}_0 - \frac{\bar{\delta}s}{2}\left(1 + \cos\frac{\Pi\bar{z}}{\bar{z}_0}\right) \quad \text{for } |\bar{z}| \le |\bar{z}_0|$$

$$= \bar{R}_0 \quad \text{for } |\bar{z}| > |\bar{z}_0| \qquad (2.1)$$

Where $\bar{R}(\bar{z})$ is the radius of the artery in the stenosis region , $\bar{R}_0$ is the constant radius of the normal artery,$\bar{z}_0$ is the half length of the stenosis and $\bar{\delta}s$ is the maximum height of the stenosis such that

$\frac{\bar{\delta}s}{\bar{R}_0} < 1,$ (for mild stenosis)

The Navier-Stokes equations governing the fluid flow is given by

$$\frac{\partial u}{\partial \bar{t}} = -\frac{\partial p}{\partial \bar{z}} - \frac{1}{\bar{r}}\frac{\partial}{\partial \bar{r}}(r\,\bar{\tau}) + \bar{F}(t) \qquad (2.2)$$

$$\frac{\partial \bar{p}}{\partial \bar{r}} = 0 \qquad (2.3)$$

Where $\bar{u}$ is the axial velocity along z-direction,$\bar{t}$ is the time, $\bar{\rho}$is the density, $\bar{p}$ is the pressure, $\bar{\tau}$is the shear stress and $\bar{F}(\bar{t})$ is the body acceleration.

For Non-Newtonian behavior of fluid, the power law model [12] is

$\bar{\tau} = -\bar{\mu}\left(\frac{\partial \bar{u}}{\partial \bar{r}}\right)^n$, where n is the power law index.

For n=2,

$$\bar{\tau} = -\bar{\mu}\left(\frac{\partial \bar{u}}{\partial \bar{r}}\right)^2 \qquad (2.4)$$

Boundary conditions are

$$\bar{u} = \bar{u}_s \quad at\ \bar{r} = \bar{R}(\bar{z})$$

$$\frac{\partial \bar{u}}{\partial \bar{r}} = 0 \quad at\ \bar{r} = 0 \qquad (2.5)$$

Where $\bar{u}_s$ is the slip-velocity at the stenotic wall[7]

We take pressure gradient as

$$-\frac{\partial p}{\partial \bar{z}}(z,\bar{t}) = A_0 + A_p \cos(\omega_p t)\ ,\ t > 0 \qquad (2.6)$$

Where A_0 represents the pressure gradient at steady state,A_p is the amplitude of the fluctuating component and $\bar{\omega}_p = 2\,\bar{\pi}\bar{f}_p(\bar{f}_p$is the pulse rate frequency).

Here A_0, A_p are two functions of $\bar{z}$ only [22].

Flow is considered under a periodic body acceleration

$$\overline{F}(\bar{t}) = a_0 \cos(\bar{\omega}_b \bar{t} + \emptyset) \qquad (2.7)$$

Where $\overline{\omega_p} = 2\pi \overline{f_b}$ ($\overline{f_b}$ is the frequency), a_0 is the amplitude and $\emptyset$ is the lead angle of the body acceleration.

To obtain the governing equations, boundary conditions and body acceleration in dimensionless form we introduce non-dimensional variables.

$$z = \frac{z}{\overline{R_0}}, z_0 = \frac{z_0}{\overline{R_0}}, \; B = \frac{a_0}{\overline{A_0}}, e = \frac{A_p}{\overline{A_0}}, t = \bar{t}\bar{\omega}_p,$$

$$R(z) = \frac{\bar{R}(z)}{\overline{R_0}}, r = \frac{\bar{r}}{R_0}, \; \omega = \frac{\bar{\omega}_b}{\omega_p}, \delta s = \frac{\bar{\delta}s}{\overline{R_0}}$$

$$u = \frac{u}{\frac{\sqrt{A_0}\sqrt{\overline{R_0}^3}}{2\sqrt{\bar{\mu}}}}, \; \alpha^2 = \frac{2\sqrt{\overline{R_0}^3}\omega_p \boldsymbol{\rho}}{\sqrt{\bar{\mu}}\sqrt{A_0}}, \tau = \frac{\bar{\tau}}{\frac{A_0 \bar{R_0}}{2}}, \qquad (2.8)$$

Where α is the pulsatile Reynolds number or generalized Womersley frequency parameter.

Using non-dimensional variables of (2.8) the basic equation of flow (2.2)and (2.4) can be written as

$$\alpha^2 \frac{\partial u}{\partial t} = 4(1 + e\,cost) - \frac{2}{r}\frac{\partial}{\partial r}(r\,\tau) + 4B\cos(\omega t + \emptyset) \qquad (2.9)$$

and

$$\tau = -\frac{1}{2}\left(\frac{\partial u}{\partial r}\right)^2 \qquad (2.10)$$

Using (2.10) the equation (2.9)can also be written alternately

$$\alpha^2 \frac{\partial u}{\partial t} = 4(1 + e\,cost) + \frac{1}{r}\frac{\partial}{\partial r}\left[r\left(\frac{\partial u}{\partial r}\right)^2\right] + 4B\cos(\omega t + \emptyset) \qquad (2.11)$$

The boundary conditions (2.5) in non-dimensional form become

$$u = u_s \qquad at\ r = R(z) \qquad (2.12)$$

$$\frac{\partial u}{\partial r} = 0 \qquad at\ r = 0 \qquad (2.13)$$

The arterial stenosis (2.1) in non-dimensional form becomes

$$R(z) = 1 - \frac{\delta s}{2}\left(1 + \cos\frac{\prod z}{z_0}\right) \quad \text{for } |z| \le |z_0|$$

$$= 1 \quad \text{for } |z| > |z_0| \qquad (2.14)$$

Volumetric flow-rate is given by

$$Q(z,t) = 4\int_0^{R(z)} r\,u(z,r,t)\,dr \qquad (2.15)$$

Where $Q(z,t) = \frac{\overline{Q}(\bar{z},\bar{t})}{\frac{\pi \overline{R_0}^4 A_0}{8\mu}}$ (2.16)

$\overline{Q}(\bar{z},\bar{t})$ is the volumetric flow rate and $\bar{\mu}$ is the viscosity.

3 Method of Solutions

Equation (2.9) and (2.10) form a system of non-linear partial differential equations. To obtain a solution we use perturbation method considering pulsatile Reynolds numberαas small parameter ($\alpha^2 \ll 1$).

We expand the velocity u in the series

$$u(z,r,t) = u_0(z,r,t) + \alpha^2 u_1(z,r,t) + \cdots \quad (3.1)$$

Substituting$u$from (3.1) in equation (2.11) and equating coefficients of α^2 and constant terms we get

$$\frac{\partial u_0}{\partial t} = \frac{1}{r}\frac{\partial}{\partial r}\left(2r\frac{\partial u_0}{\partial r}\frac{\partial u_1}{\partial r}\right) \quad (3.2)$$

$$\frac{1}{r}\frac{\partial}{\partial r}\left[r\left(\frac{\partial u_0}{\partial r}\right)^2\right] - f(t) = 0 \quad (3.3)$$

Where

$$f(t) = -4\{(1 + e\,cost) + \mathrm{B}\cos(\omega t + \emptyset)\} \quad (3.4)$$

Using the boundary conditions (2.12),(2.13) and applying the series for u of (3.1) simultaneously, we obtain the expression for u as

$$u(z,r,t) = \frac{2}{3}\sqrt{\frac{f(t)}{2}}r^{3/2} - \frac{2}{3}\sqrt{\frac{f(t)}{2}}R^{3/2} + \frac{\alpha^2 f'(t)r^3}{63\,f(t)} - \frac{\alpha^2 f'(t)R^3}{63\,f(t)} + u_s \quad (3.5)$$

Where we neglect terms of $o(\alpha^4)$ and other higher power of α.

The dimensionless volumetric flow rate and shear stress are given by

$$Q(z,t) = -\frac{4}{7}\sqrt{\frac{f(t)}{2}}R^{7/2} - \frac{2\alpha^2}{105}\frac{f'(t)}{f(t)}R^5 + 2R^2 u_s \quad (3.6)$$

$$\tau = (-1/2)[\sqrt{f(t)}\sqrt{\frac{r}{2}} + \alpha^2\frac{r^2}{21}\frac{f'(t)}{f(t)}]^2 \quad (3.7)$$

where $f'(t) = 4e\,sint + 4B\omega\sin(\omega t + \varphi)$.

4 Results and Discussions

In the present study, a mathematical model has been developed to analyze the **pulsatile blood flow** through a **time dependent stenosed arterial segment** under combined influence of **wall slip velocity** and **periodic body acceleration** considering blood as **non-Newtonian fluid**. The governing equations describing the flow dynamics were solved using **perturbation analysis** , assuming a small Womersley parameter ($\alpha < 1$) . By applying the appropriate boundary conditions, the analytical expression for the **velocity profile**, **wall shear stress** and **volumetric flow rate** were derived.

To evaluate the applicability of this model , the variation of **velocity (u) ,flow rate (Q), wall shear stress (τ)** were numerically estimated and presented in graphically . To assess the impact of slip-velocity , the values of u_s were taken from 0.5 to 0.9. To examine the effect of body acceleration on blood flow in the constricted artery body acceleration parameter was varied from 0.0 to1.0.Maximum stenosis height was taken as 0.6.

Figure 2 and **Figure 3** illustrate that as the **slip velocity u_s** increases , the **volumetric flow rate (Q)** increases almost linearly while an increase in **Womersley parameter (α)** causes a gradual decrease in **Q** .

From **Figure 4** it is observed that **pressure gradient** increases with time up to a certain point, remain constant over an interval and then decreases at the rate in which it increased.

Figure 5 shows that shear stress increases linearly with radial position (**r**)for all values of **Womersley parameter (α).**

Figure 6 shows that the **velocity(u)** decreases progressively as **stenosed radius (R)** increases. This implies that blood flow slows down and eventually reverses near the **constricted arterial wall**.

From **Figure 7**, it is evident that increasing the **Pressure gradient parameter (e)** leads to an increase in **shear stress** for different values of r. **Figure 8** shows the effect of **body acceleration parameter (B)** on **volumetric flow rate (Q)** for different values of R . It is observed that when $0.2<R<0.5$,**Q** decreases slowly with increasing **B**. However, for $R>0.5$, **Q** decreases sharplyas **B** increases .

Figure 9 reveals that in the stenosed region , **the volumetric flow rate (Q)** decreases as the radius (**R**) approaches the arterial wall for different values of **B** . Conversely, near the **centre line** ($R<0.7$), **Q** increases with increasing **B**.

As shown in **Figure10, Q** decreases gradually as **R** approaches 1 in the stenosed region for different values of e. However, when $R\leq0.6$ i.e near the central axis of the stenosed artery, Q increases with e.

Finally, **Figure 11** demonstrate that at R=0.5 the **velocity(u)** corresponds the **slip velocity us**. For different values of **R**, the velocity increases when $120<t<180$, while it decreases in the range $180<t<240$.

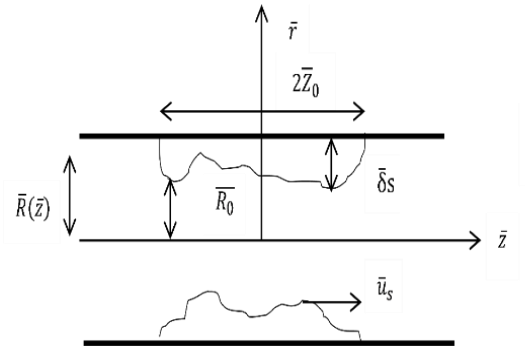

Figure 1

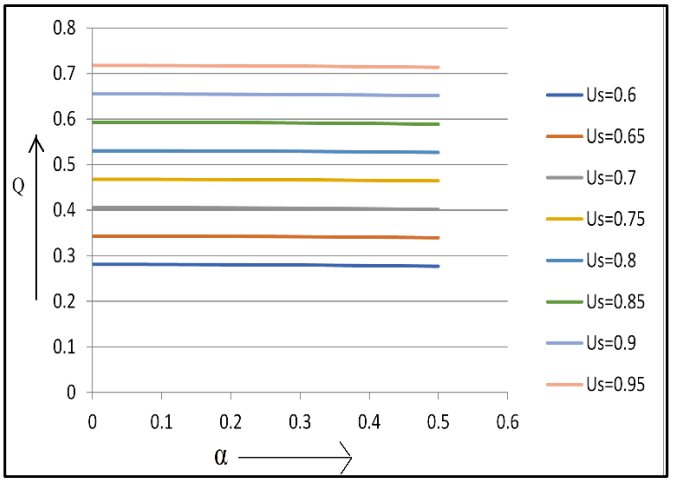

Figure 2

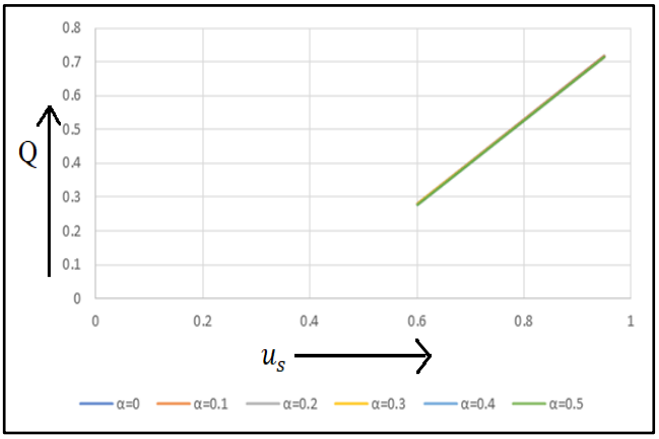

Figure 3

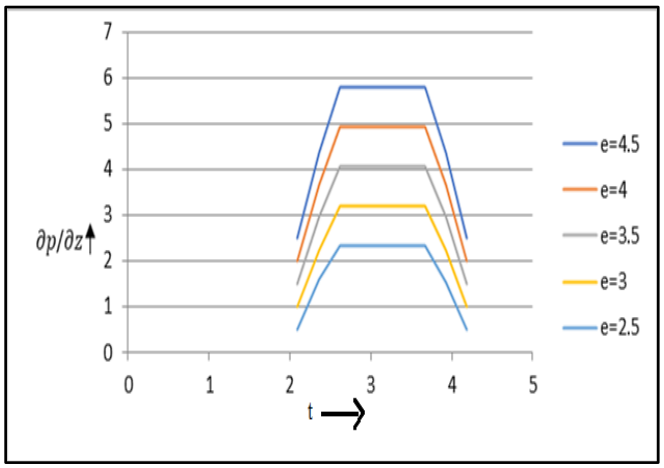

Figure 4

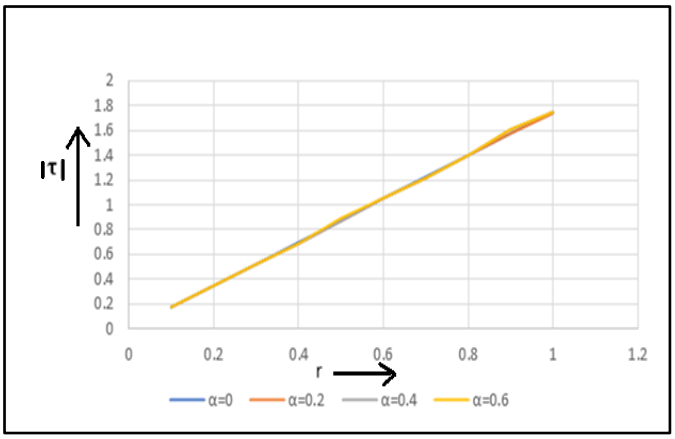

Figure 5

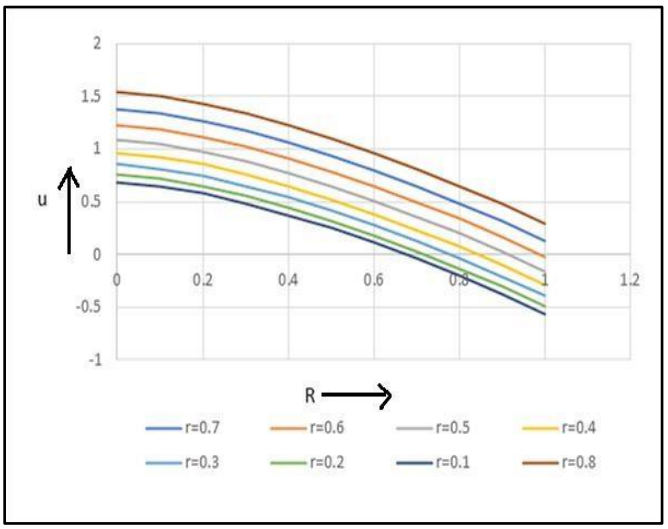

Figure 6

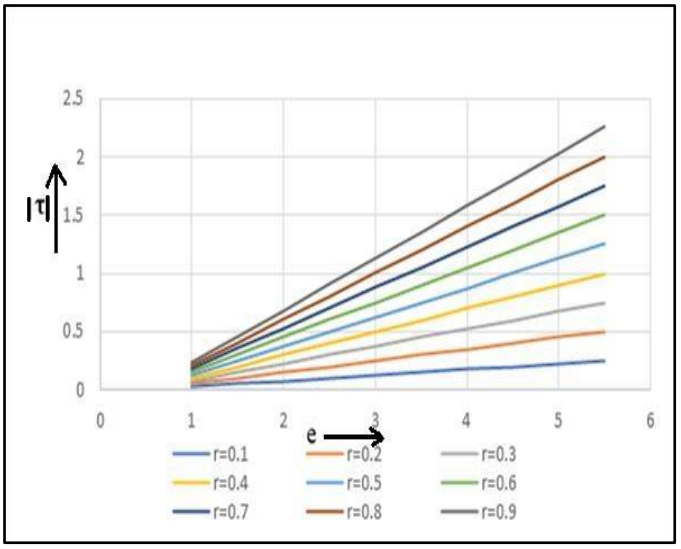

Figure 7

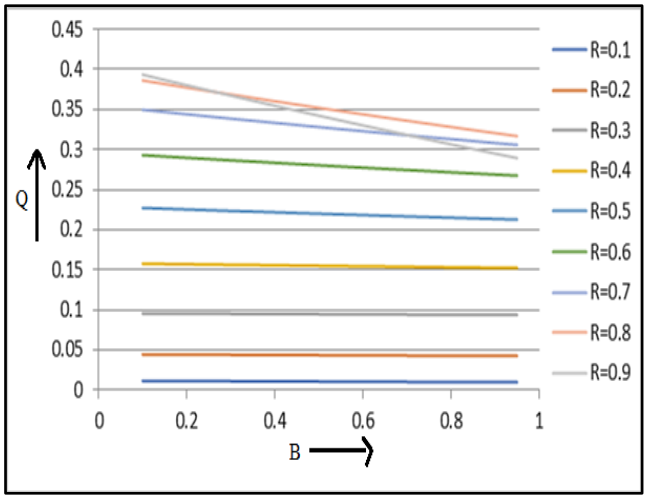

Figure 8

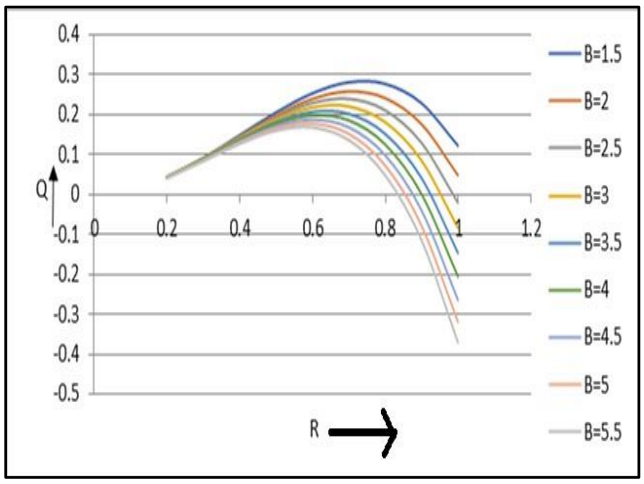

Figure 9

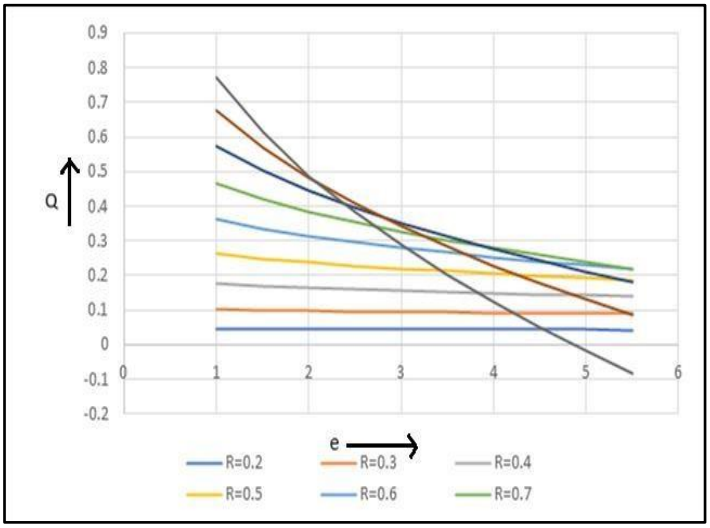

Figure 10

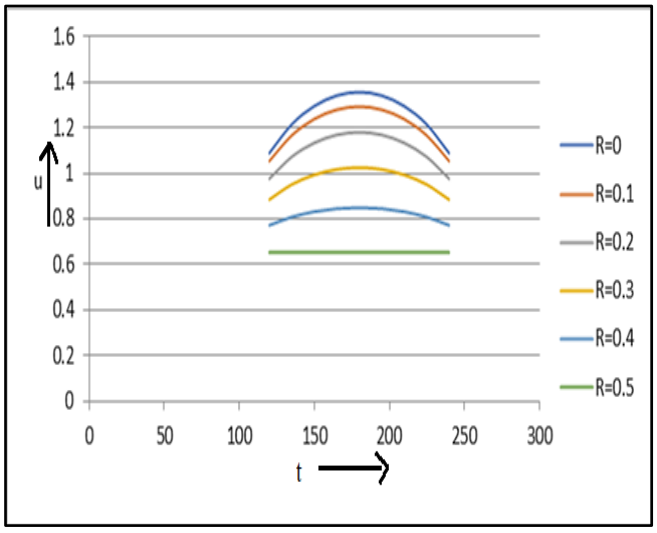

Figure 11

Conclusion

To investigate the blood flow through a narrow stenosed artery, we model blood as a **non-Newtonian fluid**. To represent this behavior effectively , we adopt a simplified constitutive relation as describes in equation (2.4). After **non - dimensionalizing** the governing equations and boundary conditions , the resulting system of **nonlinear partial differential equation** is solved by using the **perturbation method**.

Our analysis reveals that the **slip velocity** at the arterial wall and **periodic body acceleration** significantly influence the blood flow characteristic in a stenosed artery when the **non-Newtonian** nature of blood is taken into account. Notably, it is observed that with an increase in body acceleration, the **velocity flux** decreases considerably and may even approaches zero and direction of velocity reverse near the constricted wall of the stenosed region -particularly under moderate **wall shear stress** conditions. **Wall-slip** increases the **velocity of blood flow** and **volumetric flow rate**. Enhancing **slip at the arterial wall** can help to **increase blood flow** in the stenosed region .

References

[1]F.R.Eirich, Rheology Theory and Applications, Vol. 3, Academic Press Inc. Publishers, New York, S.F.London, 1960.

[2]G,B,Thurston : Viscosity of Human blood Biophys. J 12 (1972) 1205 -1217

[3]A.C . Arntzenius, J.D. Laird,A. Noordergiaal , P.D.Verdouw, P.H. Huismanm Body Acceleration

Synchronous with Heartbeat, Biophy.Cardio.29 (1972) 1-5

[4] G,B,Thurston : Frequency and Shear Rate Dependence of Viscoelasticity of Human Blood Biorheol [O (1973)375 -381.]

[5] Young D.F. (1979) "Fluid Mechanics of Arterial Stenosis." Journal of Biomechanics Eng .ASME, Vol.101, pp 157-175

[6] Chien, S.,Hemorheology in clinical medicine,Recent Advances in Cardiovascular diseases 2(Suppl)(1981) , 21-26.

[7] Chaturani,P. and Biswas D.(1984) : A Comparative study of Poiseulle flow of a polar fluid under various boundary conditions with application to blood flow,Rheol,Acta.Vol.23,pp 435 – 445.

[8]J.N.Kapur (1985): Mathematical Models in Biology and Medicine, New Delhi;East-West Press

[9]L.M.Srivastava (1985), "Flow of couple stress fluid through stenotic blood vessels, Journal of Biomechanics, Vol.18, No.7, pp 479-485

[10]Sud and G.S.Sekhon(1985) Arterial flow under periodic body acceleration Bulletin of Mathematical Biology Vol 47,No.1,1985,pp 35-52.

[11] S.Chakraborty (1987) " Effect of Stenosis on the Flow of Blood in an Artery.International Journal of Engineering Science , Vol. 25,No.8, pp 1003-1016

[12]J . Majumdar (1989) An Introduction to Mathematical Physiology & Biology, Cambbridge University Press.

[13]]P.Chaturani,V.Palanisamy (1991) Pulsatile Flow Of blood with body Acceleration Int. J. Eng. Sci 29 , 113-121

[14]P.Chaturani,V.Palanisamy (1990) Casson fluid model of pulsatileflow of blood under periodic body acceleration .Biorheol.27.

[15]A.R.Pries,D.Neuhaus and P,Gachtegnes (1992) " Blood viscosity in Tube flow:Dependence on Diameter and Hematocrit"American Journal of Physiology,Vol263 pp 1170-1178 .

[16]V.K.Verma, M.P.Sing and Dr.V.K.Katiyar (200 Analytical study of blood flow through an artery with mild stenosis , ActaCienciaIndiceVol.XXXM(2),281

[17]J.C.Misra and G.C.Shit, "Blood flow through arteries in a pathological state; a theoretical study." International Journal of EngineeringScience , Vol. 44,No.10, pp 662-671,(2006)

[18]R.Bali and U.Awasthi(2007) Effect of a magnetic field on the resistance to blood flow through stenotic artery, Applied Mathematics and Computations 188. 1635-1641

[19]Sankar D.S.,Lee U. Mathematical Modelling of pulsatile flow of non-Newtonian fluid in stenosed arteries ,commun. Nonlinear Sci Mumer.Simulat.2009 ; 14; 2971-81.

[20]Misra J.C. and Shit G.C. (2007) : Role of slip velocity in blood flow through stenosed arteries : A non- newtonian model, Journal of Mechanics in medicine and Biology. Vol-7 ,p 337-353.

[21]R.Ponalagusamy(2007),Blood flow through an artery with mild stenosis: a two-layered model, different shapes of stenosis and slip velocity at the wall", Journal of Applied Sciences, vol 7.no.7pp 1071-1077.

[22]P.Nagarani and G.Sarojamma(2008) " Effect of body acceleration on Pulsatile flow of casson fluid through a mild stenosed artery ", Korea Australia Rheology Journal, Vol 20,no.hpp 189-196.

[23]V.P.Srivastava and R Srivastava , (2009) " particulate suspensionBlood Flow Through a Narrow Catheterized Artery",Computers and Mathematics with Applications ,Vol. 58,No.2,pp 227-238

[24] Sankar,D.S. and Lee .U.(2009). Mathematical Modelling of Pulsatile flow of Non-newtonian fluid in stenosed arteries .Common Non-linear Numer simulat. Vol 14.pp2971 -2981.

[25] Biswas D. Chakraborty US . Pulsatile blood flow in a constricted artery with a velocity slip .Far East J Appl.Math. 2009; 36: 331 -42.

[26] Kumar S and Diwakar C.S. (2013) : A mathematical Model of Power Law Fluid with an Application of Blood flow through an artery with stenosis , Advances in Applied Mathematical Bioscience Vol. 4, No. 1 (2013) pp 25-36

[27]M.G. Rabby, A.Razzak,Md. M.Molla, Pulsatile non-Newtonian blood flow through a model of arterial stenosis , Procedia Engineering 56 (2013)225-231

[28]Sanyal .M.K. Pulsatile flow of blood in an Elastic tube with Slip at the Wall ,J.Mech.cont.&Math Sci, vol-11, No.1,(2016)

Approaches for synthesis, characterization, doping and prospective applications of graphene quantum dots

Madhurima Chakraborty[1] and Tapan Ganguly[2]

[1] Department of Biochemistry, West Bengal State University, Kolkata 700 126, India

[2]School of Laser Science and Engineering, Jadavpur University, Kolkata 700032, India

[2] Email: tapcla@rediffmail.com

1 Abstract

Carbon dots have become popular in the last few decades owing to their small size, low toxicity and biocompatibility, simple functionalization strategies, eco-friendly synthesismethods and many others. Among the carbon dot family, Graphene quantum dots (GQDs) have been extensively studied in recent years due to its particular structural, optical, electrical, surface modification, biofunctionalization and optoelectrical properties enabling its prospective biomedical application. The exceptional characterisitics of GQDs such as photoluminescence, multi-color emission, photo-stability, biocompatibility, small size are mostly derived from the quantum confinement effect and edge effect. Keeping the structural and functional aspects of GQDs, the focus of the review is to outline the possible strategies of synthesis of GQDs, the various ways to characterise the synthesized GQDs, doping with various heteroatoms and an outline of the technological application.

2 Introduction

In the last few decades, immense focus has been given on the optoelectronic properties of nanostructured semiconductors or quantum dots (QDs). After the discovery of graphene in the year 2004 [1], metal-free carbon-based QDs like carbon QDs (CQDs), graphene quantum dots (GQDs), and graphitic-carbon nitride QDs (g-CNQDs), have emerged as potential candidates having the ability to substitute and replace the conventional metallic QDs [2-4]. On one handcarbon-based QDs own good physicochemical properties likegood stability and tunable fluorescence of metallic QDs, and on the other hand they also possess unique characteristicslike ease of synthesis, brilliant biocompatibility and nontoxicity. [5-15]

GQDs, one of the recently discovered carbon-based nanomaterials, are derived from two-dimensional graphene, which limits electronic transport in all three spatial dimensions [16-18]. GQDs are small enough to confine excitons. They are known to have a diameter of less than 20 nm and have a non-zero band gap. Compared with carbon nanodots, GQDs have good chemical and physical attributes, namely, a greater length-to-diameter ratio, higher surface area, and better surface bonding through the double π–π network due to their graphene layer structure. Additionally, as already mentioned, GQDs exhibit an attractive property called photoluminescence, which can be attributed to quantum confinement [19-22].

Ever since the discovery of fullerenes in the year 1985, functional materials of crystalline allotropes of carbon have gatheredimmense interest in materials science, biophysicsand biotechnology. Accordingly, one carbon allotrope particularly graphene, comprise of highly-ordered and closely packed monolayer of single two-dimensional sheet of carbon atoms bonded to form a hexagonal lattice. This confers distinctivecharacteristicslike zero-energy bandgap thatoccursbecause of the overlapping of the valence and conductance bands. When the electronic structure is altered by restricting physical dimensions of graphene

to finite values and defects getsadded within the lattice, the non-zero values of energy bandgaps are witnessed [23-25].Relevantly, the quantum confinement effects of graphene sheets enable tunabilityof the bandgap and size control of graphene therebyallowingapplications in optoelectronics, energy harvesting and nano-medicine [26, 27].Moreover, since,GQDsare usually obtained by converting two-dimensional graphene to zero-dimensional material [28], therefore,this leads toreduced dimension of the crystal to nanometer scale by modification of electron distribution. These properties are mostly responsible for providingquantum confinement and edge effects of GQDs. Due to the quantum confinement effect,GQDs possess unique fluorescent properties as discovered in 2010 by Pan et al [29]. Besides, the enhanced solubility of GQDs due to the large edge effect can be modulated by dopants.Moreover, modification of properties of GQDs by means of doping with nitrogen was first reported in 2012by Zhao [30] and his groups.

Along with quantum confinement and edge effects, GQDs possess many notableproperties like stable good solubility, photo-luminescence, biocompatibility, surface functionalizationand inertness [31]. Some of these properties are seeminglybetter compared to conventional semiconductor quantum dots, that enable potential applications of GQDs especially in the fieldsof drug-carriers [32-37],bio-imaging [38-41], photo-detectors [42-47], fluorescent agents [48-51], light-emitting diodes [52] (LEDs) and sensors [53,54] and others.The specialphysicochemicalcharacteristics of GQDs are results of theproperties like quantum confinement and edge effects and based on these properties, numerous applications are employed.

Accordingly, the review focuses on synthesis and doping strategies of GQDs. Methods tocharacterize the synthesized GQDs are also outlined. Lastly, the technology based applications are overall discussed.

3 Synthesis strategies for graphene quantum dot

GQDs are known to possess various chemical and physical properties in comparison to carbon dots, carbon nanotubes and fullerenes mainly due to its specificedge and quantum confinement effects. Also, the physicochemical properties of nanomaterials are oftenregulatedby the synthesis and fabrication methods to be employed. Methods to synthesize GQDs can be classified into two waysbased on the precursor component to be used. The common strategies include top-down and bottom-up approaches.

Top-down method follows cutting of graphene-related materials like graphene, graphene oxide, carbon nanotubes, carbon fibers, carbon black, graphite powder and coal etc. into quantum sizeusing liquid exfoliation, electron beam lithography techniques and othertechniques. This approach is advantageous due to plentiful raw materials and the processes often produce oxygen-containing functional groups at the edge, therebypromoting their functionalization, solubility andbiocomptability. However, some disadvantages, like low yield, size defects and non-controllability of shape and size and may be others [2, 55, 56].

In bottom-up approach, GQDs are formed by growthofprecursor moleculeslike benzene, phenol compounds, glucose, citric acid and fullerene and others into nano-sized GQDs using hydrothermal, microwave-assisted hydrothermal, soft-template and metal-catalyzed methods and others. This approach is beneficial, because of lesser defects and controllable size and shape. On the other hand, reduced solubility, aggregation and small size are some of the disadvantages of this approach [57-70].

3.1 Bottom-up methods

As already mentioned, bottom-up approaches usually follow growth of molecular precursorsthat may be graphene-like smaller polycyclic aromatic hydrocarbons (PAHs) or other molecules stated above into GQDs. Accordingly, based on the way external energy can

be provided,this strategy can be sectioned into four main methods. The methods are hydrothermal, microwave-assisted hydrothermal, soft-template and metal-catalyzed methods.

3.1.1 Hydrothermal method

Briefly, this method involves techniques for crystallizing substances from high-temperature aqueous solutions to high vapor pressures. The fabrication of single-crystalline GQDs through this method has been demonstrated by numerous researchers [70, 71].

3.1.2 Microwave-assisted hydrothermal method

Hydrothermal synthesis of GQDs is often time-consuming and may not be suitable for large-scale industrial production. Therefore, a fast and effective method is needed to bedeveloped. This may be achieved by the help of microwave-assisted hydrothermal (MAH) method [72-74]. Using microwave irradiation the duration of growth of GQDs may be lessened to minutes or even seconds.

3.1.3 Soft template method

A novel method, known as soft-template, isemployedfor easy, cheap and nature friendly fabrication of GQDs. This method facilitates nanoscale reaction cavity and the separation and purifying processes are relatively simple and thus can be used for large scale production [75, 76].

3.1.4 Metal-catalysed method

Metal-catalysed method is a less practised route for synthesis of GQDs. Loh et al. [77] utilized ruthenium as metal catalyst and C60 as a precursor to synthesize GQD. By controlling the annealing temperature the shape and morphology of the GQDs could be modulated.The GQDs synthesized through these methods are sometimes soluble only in organic solvents, which may restrict biological applications of GQDs.

3.2 Top-down methods

As already mentioned, top-down method are carried out by cutting of graphene-related materials into quantum size by liquid exfoliation, electron beam lithography techniques and other techniques.

3.2.1 Liquid exfoliation method

Nowadays liquid-phase exfoliation is frequentlyapplied for the synthesis of grapheme. Here intercalation of graphite iscarried outby strong oxidizing agents. This is followed by expansion of graphite layers via thermal or chemical methods. This approach has been also used in the synthesis of GQDs by researchers [87-91]. The preparation of GQDs oftenneeds the treatmentwith acid for the cutting of graphene.

3.2.2 Electrochemical Exfoliation

In this method, layered bulk materials, like graphite rods, are exfoliated using an applied electric field. Earlier this method was used to produce pristine graphene sheets, [82,83], but now electrochemical exfoliation has also been used to prepare GQDs with specific control over size and morphology. Here, sp^2 hybridized carbonmaterials, like graphite or multiwalled carbon nano tubes, go througha two-step process: firstly the sp^2 hybridized carbonmaterial is placed in an electrolyte solution. Then an anodic potential is employedwith respect to a reference electrode thus, beginning sp^2bondcleavage and intercalation of the solvent molecules within layers of bulk material.Secondly,for electrochemical reduction of the product a cathodic potential is applied. [84] This controlled applied electric potential supportsregulatedoxidation within the bulk material, in contrast to other methods, where oxidation cannot be controlled. Moreover, this method does not need toxic oxidizing / reducing agents and thus can be carried out under ambient conditions.

3.2.3 Ultrasound assisted method

Ultrasonic assisted method is anotherstrategy formaterial synthesis [78, 79]. In presence of ultrasound the mechanical force producedmay break the carbon–carbon bonds, thus cutting and producing GQDs.

3.2.4 Laser ablation

The methoduses higher-energy laser pulse to irradiate the surface of the target, resulting in increase of temperature andpressure, heat generation and evaporation, and converting them to plasma state. Then, the vapor iscollected and crystallized into quantum dots [80].

4 Characterization of synthesized graphene quantum dots

Different methods are performed to understandthe structural morphology and composition of particles based on how they are synthesized and regardless of their probable usage. As already discussed that GQDs possess particular optical and physicochemical properties, and such properties are needed to be recognized and linked to variousmonitoring experiments. The probable techniques include High-resolution transmission electron microscopy (HRTEM), X-ray diffraction (XRD), atomic force microscopy (AFM),UV-vis, fluorescence studies, Raman spectroscopy,X-ray photoelectron spectroscopy (XPS) and infrared spectroscopy (FTIR) for analysing crystal structures and surface morphology fluorescence properties, electronic states, vibrational patterns and functional group composition respectively.

4.1 High-resolution transmission electron microscopy (HRTEM)

HRTEM offers the possibility of visualizing GQDs and provides the information about the distribution, shape of particles, crystallinity, and edge types. The observations from HRTEM can be confirmed with XRD data [81].

4.2 X-ray diffraction (XRD)

XRD is an importanttool for understanding the amorphous or crystalline phase and determining the level of crystallinity, and the distribution of particle size of numerous nanoparticles. It is particularly noteworthy in attainingfruitfulknowledge about the atomic arrangement anddimensions of the unit cells. The XRD pattern of the GQD usuallyshows a broad peak located near $2\theta = 25°$, which possibly indicate that the material is composed of an irregular arrangement and disorganization due to oxygen molecules with functional groups [82, 83].

4.3 Atomic force microscopy (AFM)

AFM is a versatile and powerful microscopic technique which gives insights into the surface topography of the sample. It is commonly used to investigate the thickness/ height of GQDs and to further estimate the number of graphenelayers. The thickness noted for GQDs usually ranges upto 1-3 nm suggesting few layers of graphene oxide like structure [84].

4.4 UV-vis spectroscopy

UV-vis absorption studymonitors the electronic transitions of materials in UV- visible range. In aqueous solution, UV-vis absorption spectra ofGQDs show peaks in the UV region associated with a tail extending to the visible range. The observations may be commonly attributed to π–π^* transition of the C=C bonds and n–π^* transition of C=O bonds [85].

4.5 Fluorescence spectroscopy analyses

Fluorescence spectroscopy experiments assess fluorescence or photoluminescence (PL) from a sample. When GQD samplesare excited at particular excitation wavelength, the GQDs emit corresponding emission peaks. Studies so far reveal that GQDs demonstrate either excitation-dependent or excitation-independent emission in different colour regions of emission light like blue, green, yellow, cyan or red. The emission properties of GQDs are related to probably their highly defective structures with sp^3 and vacancy defect states in the basal plane [85].

4.6 Raman spectroscopy

Raman spectroscopy is animportant technique that gives knowledge regarding molecular vibrations and is used for characterising nanomaterials speciallygraphene. It usually depictsaspectsoflattice vibrations,electronic structure, surface defectsand crystal structure of nanomaterials. Bands inRaman spectra of carbon-based materials like GQDs and nanotubes, possess systematic variations and represent the defect (D band) and tangential (G band) modes. The G peak near 1570 cm^{-1}suggests good crystallinity of GQDs and is associated to sp^2 vibration on the carbon plane. The D peak near 1380 cm^{-1} isassociated with sp^3 hybridized carbon atomsrelated to defect states in GQDs owing to multiple edge effects.The relative intensity of the “disorder” D band to the crystalline G-band (ID/IG) for the GQDs is usually observed to be close to 1, which probably suggests that GQDspossess high crystallinity and disorder within the skeleton [84, 86].

4.7 X-ray photoelectron spectroscopy (XPS)

XPS is a very effective technique that is used to assess the surface elemental chemistry of nanomaterials. The elemental composition and oxidation state of the element

present at the surface of the materials are obtained from XPS. It is mostlyperformed along with FT-IR to understand the material components and functional groups [86, 87]

4.8 Fourier transform infrared spectroscopy (FTIR)

FTIR is a useful method for detecting surface components and functional groups on materials in a qualitative manner. As IR radiation is applied tothe sample, some of the radiation is absorbed by molecular vibrations and the rest is transmitted. The molecular vibration state gives a characteristic signal for each molecule, which is utilized to inspect functional groups present in GQDs. The FTIR result are represented by notable vibrational peaks like- C=C stretching related peak near 1580 cm^{-1}, O–H related peak near 3400 cm^{-1}, C–H related peaks near 2976 and 1376 cm^{-1} and C–O related peak near 1206 cm^{-1}[85-88] .

5 Functionalization of graphene quantum dots

In order to expand thewide-range of application of GQDs in a variety of fields, the GQDs are functionalized by different methods to tailor its properties for particular applications. Functionalization of GQDs can modify theelectronic,optical and chemical properties, enabling potential biomedical applications. Functionalization usually includes doping with heteroatoms, formation of composites with inorganic materials or polymers and adjustingthe size and morphology of GQDs. Research related to the functionalization of GQDs is an emerging area in the study of nanomaterialsof carbonnanofamily.

Effective doping can regulatethe electronic,optical and chemical properties of GQDs. It is possible to characterize the effect of doping, for example, by determining the change in the color of PL, the conductivity and water solubility of the doped GQDs. Heteroatoms used in the doping of GQDs include nitrogen (N), phosphorus (P),sulphur (S), boron (B), oxygen (O), selenium (Se), chlorine (Cl),fluorine (F),sodium (Na)andpotassium (K).Mostly, the doping method can be grouped into three categories depending on the number of atomsto be

doped. The atoms can bedoped withsingle andco-doped with double and multiple heteroatoms within GQDsas well,thus, enabling and enhancingspecific properties of GQDs [2, 56, 89-94].

6 Prospective biomedical and technological applications of graphene quantum dots

While much of the current research is focused on improving optical properties of GQDs, biocompatibility remains an important aspect for in vivo applications of these materials. The scope of the biocompatibility of a material is subject to a specific application; however, the overarching definition of biocompatibility is the ability of the material to perform its intended function without inducing unintended biological reactions.[53] Although toxicity due to aggregation has been reported in many carbon-based nanoparticles, GQDs display excellent solubility in water and provide a non-toxic alternative to metal-based nanoparticles by eliminating the toxicity concern due to metallic residues that are not cleared from the body since GQDs are entirely composed of carbon.

The GQDs possess unique optical properties which help to develop various opto-electronic devices [95, 96]. This is primarily based on some special characteristics of GQDs, which are upconversion, strong photoluminescence and tuning of energy gap by controlling size/shape, which are different from traditional quantum dots. There are many potential applications of GQDs in the optical field. Photodetectors are sensors of light or electromagnetic radiations which play an important role in space exploration, national defense and real-time monitoring. The outstanding optical properties of GQDs have been used to coating LEDs with GQDs to do modifications in its lighting intensity and emitting wavelength. GQDs also act as a phosphors being coated on to the surface of LEDs, which helps to transform of color as well as augmentation in intensity of emitting lights.

Another important application is in production of renewable energy source. This can be made by carbon materials, which are low-cost, abundant, environmentally friendly, biocompatible and biosafe and have been investigated as photocatalysts [97] for cost-effective hydrogen production. GQDs show up as the best candidate for photocatalysis applications, among the carbon materials, due to its many marvelous properties.

As the resources of our earth gradually becoming limited whereas growth of population is on rise it becomes a life-threatening situation and urgent researches to explore new and sustainable energy for the future become very important. As carbon is one of the most plentiful materials in the world, it can be considered as an excellent candidate for energy-related applications.

Solar cells, which covert sunlight to electricity, provide clean and renewable energy source [98]. It is also an essential energy source for society which has limited resources to generate electricity using conventional methods. The characteristics of GQDs, such as the down-conversion, strong fluorescence, intensive absorption at UV range and easily-functionalization etc., have led to development of different solar cells using GQDs to enhance significantly the performances of the cells. Though still some of the solar cells were based on traditional silicon solar cells, significant researches are going on to build the hybrid of Si and GQD solar cells, polymer solar cells, dye-sensitized solar cell (DSSC) and other novel solar cells etc.

The biocompatible and high-performance battery is composed of GQDs and the GQDs play vital role in the enhancement of battery performances.

Fuel cell[99] can generate electricity through an electrochemical reaction of hydrogen fuel with oxygen. Such energy technology is sustainable and environmentally friendly. Recent studies have demonstrated the use of functionalized GQDs as fuel cell electrodes.

Recent time resolved spectroscopic studies on some short-chain dyad-GQD nanocomposite systems show the properties of artificial light energy conversion materials and energy storage systems. It was seen in these nanocomposite devices the role of GQD is very important to enhance the efficiency of the energy storage ability.

GQDs are progressively becoming imperative functional materials that possess applications in single-electron transistors, organic-inorganic solar cells, LEDs, lasers, single-photon sources, second-harmonic generation (SHG), quantum computing, cell biology research, microscopy, and medical imaging. medical, optical and energy-related fields. However, understanding of the mechanism in some of the GQDs applications remains imprecise and requires further investigations to explore the exact nature.

7 Acknowledgements

MC expresses her gratitude to laboratory grants from West Bengal State University. TG thanks School of Laser Science and Engineering, Jadavpur University for supporting research work.

8 References

[1] X Y Xu, R Ray, Y L Gu, H J Ploehn, L Gearheart, K Raker, W A Scrivens, J. Am. Chem. Soc. 126 (2004) 12736-12737.

[2] P Tian, L Tang, K S Teng, S P Lau, Materials Today Chemistry 10 (2018) 221-258

[3] S Chung, R A Revia, M Zhang, Adv Mater. 2021 June; 33(22)

[4] C Zhao, X Song, Y Liu, Y Fu, L Ye, N Wang, F Wang, L Li, M Mohammadniaei, M Zhang, Q Zhang, J Liu, J Nanobiotechnol (2020) 18:142

[5] S Bak, D Kim, H Lee, Curr Appl Phys. (2016) 16:1192–201.

[6] P Zheng, N. W, Chem An Asian J. (2017) 12:2343–53.

[7] Y Du,S. Guo, Nanoscale. (2016) 8:2532–43.

[8] Y Yan, J Gong, J Chen, Z Zeng, W Huang, K Pu, J Liu, P Chen,Adv Mater.(2019) 31:e1808283.

[9] H Singh, S Sreedharan, K Tiwari, N H Green, C Smythe, S K Pramanik, J A Thomas, A Das,ChemCommun. (2019) 55:521–4.

[10] X Li, H Guo, S Ren, R Fan, Y Yu, H Zhang, C Liu, L Miao,ApplBiochemBiotechnol. (2019) 47:115–22.

[11] C Qu, D Zhang, R Yang, J Hu, L Qu,SpectrochimActa A MolBiomolSpectrosc.(2019) 206:588–96.

[12] W Chen, G Lv, W Hu, D Li, S Chen, Z Dai, Nanotechnol Rev. (2018) 7:157–85.

[13 D Cui, F Tian, CS Ozkan, M Wang, H Gao,ToxicolLett. (2005) 155:73–85.

[14] Y Xie, B Wan, Y Yang, X Cui, Y Xin, LH Guo, J Environ Sci China. (2019) 77:198–209.

[15] F Nasrollahi, YR Koh, P Chen, J Varshosaz, AA Khodadadi, S. Lim, Mater SciEng C. (2019) 94:247–57.

[16] K S Novoselov, AK Geim, SV Morozov, D. Jiang, Y Zhang, SV Dubonos,IVGrigorieva, AA Firsov, Science. (2004) 306:666–9.

[17] L Jiao, L Zhang, X Wang, G Diankov, H Dai, Nature. (2009) 58:877–80.

[18] DV Kosynkin, A L Higginbotham, A Sinitskii, J R Lomeda, A Dimiev, BK Price, JM Tour, Nature. (2009) 458:872–6.

[19] D Pan, J Zhang, Z Li, M Wu,Adv Mater (2010) 22:734–8.

[20] S Dorontic´, S Jovanovic´, A Bonasera, Materials, (2021) 14, 6153.

[21] M Bacon, S J Bradley, T Nann, Part. Part. Syst.Charact., (2014) 31, 415–428.

[22] S Zhou, H Xu, W Gan, Q. Yuan, RSC Adv., (2016) 6,110775–110788.

[23] L Li, G Wu, G Yang, J Peng, J Zhao, JJ Zhu, Nanoscale(2013) 5, 4015.

[24] K L Schroeder, R V Goreham, T Nann, Pharm. Res (2016) 33, 2337.

[25] V Borse, M Thakur, S Sengupta, R Srivastava, Sens. Actuators B Chem(2017) 248, 481.

[26] S Kundu, V K Pillai, Phys. Sci. Rev., (2020) 5, 20190013.

[27] J Shen, W Chen, Z Yang, G Lv, J Cao, D Li, X Liu,NANO, (2021) 16, 2130001.

[28] D Wang, JF Chen, L Dai, Part. Part.Syst. Char (2015) 5515-523.

[29] D Pan, J Zhang, Z Li, M Wu, Adv. Mater. (2010) 6 734-738.

[30] YZhao, CG Hu, Y Hu, HH Cheng, GQ Shi, LT Qu, Angew. Chem. Int. Ed. (2012)5111371-11375.

[31] SY Lim, W Shen, Z Gao, Chem. Soc. Rev. (2015) 44 362-381.

[32] X Yao, X Niu, K Ma, P Huang, J Grothe, S Kaskel, Y Zhu, Small (2017) 2 1602225.

[33] Z Wang, J Xia, C Zhou, B Via, Y Xia, F Zhang, Y Li, L Xia, J Tang, Colloids Surfaces B Biointerfaces (2013) 112 192-196.

[34] H Chen, Z Wang, S Zong, P Chen, D Zhu, L Wu, Y Cui, Nanoscale(2015) 7 15477-15486.

[35] H Ding, F Zhang, C Zhao, Y Lv, G Ma, W Wei, Z Tian, ACS Appl. Mater. Interfaces (2017) 33 27396-27401.

[36] J Dong, K Wang, L Sun, B Sun, M Yang, H Chen, Y Wang, J Sun, L Dong, Sensor. Actuator. B (2017) 256 616-623.

[37] J Qiu, R Zhang, J Li, Y Sang, W Tang, PR Gil, H Liu, Int. J.Nanomed. (2015) 10 6709-6724.

[38] H. Shen, L. Zhang, M. Liu, Z. Zhang, (2012) 3 283-294.

[39] K Li, W Liu, Y Ni, D Li, D Lin, Z Su, G Wei, J. Mater. Chem. B (2017) 5 4811-4826.

[40] PC Wu, JY Wang, WL Wang, CY Chang, CH Huang, KL Yang, JC Chang, CLL Hsu, SYChen, TM Chou, WS Kuo, Nanoscale(2018) 1 109-117.

[41] S Zhu, J Zhang, C Qiao, S Tang, Y Li, W Yuan, B Li, L Tian, F Liu, R Hu,H Gao, H Wei, H Zhang, H Sun, B Yang, Chem. Commun. (2011) 24 6858.

[42] T Yu, F Wang, Y Xu, L Ma, X Pi, D Yang, Adv. Mater. (2016) 24 4912-4919.

[43] G Haider, P Roy, CW Chiang, WC Tan, YR Liou, HT Chang, CT Liang,WH Shih, YF Chen, Adv. Funct.Mater. (2016) 4 620-628.

[44] CW Chiang, G Haider, WC Tan, YR Liou, YC. Lai, R Ravindranath, HT Chang, YF Chen, ACS Appl. Mater. Interfaces(2016) 1 466-471.

[45] G Konstantatos, M Badioli, L Gaudreau, J Osmond, M Bernechea,FPG Arquer, F Gatti, FHL Koppens, Nat. Nanotechnol. (2012) 6 363e368.

[46] Q Zhang, J Jie, SDiao, Z Shao, Q Zhang, L Wang, W Deng, W Hu, H Xia, X Yuan, ST Lee, ACS Nano (2015) 2 1561-1570.

[47] H Tetsuka, A Nagoya, SI Tamura, Nanoscale (2016) 47 19677-19683.

[48] L Zhou, F Wu, J Yu, Q Deng, F Zhang, G Wang, Carbon (2017) 118 50-57.

[49] M Mehrzad-Samarin, F Faridbod, AS Dezfuli, MR Ganjali, Biosens. Bioelectron.(2017) 92 618-623.

[50] P Nuengmatcha, P Sricharoen, N Limchoowong, R Mahachai, S Chanthai, RSC Adv. (2018) 8 1407-1417.

[51] Q Xu, Q Zhou, Z Hua, Q Xue, C Zhang, X Wang, D Pan, M Xiao, ACS Nano (2013) 12 10654-10661.

[52] D Raeyani, S Shojaei, S Ahmadi-Kandjani, Superlattice. Microst. (2018) 114 321-330.

[53] SH Song, MH Jang, J Chung, SH Jin, BH Kim, SH Hur, S Yoo, YH Cho, S Jeon, Adv. Opt. Mater.(2014) 11 1016-1023.

[54] S Benitez-Martinez, M Valcarcel, Sensor. Actuator. B Chem. (2014) 197 350-357.

[55] F Chen, W Gao, X Qiu, H. Zhang, L Liu, P Liao, W Fu, Y Luo, Frontiers in Laboratory Medicine (2017) 1 192–199

[56] N Sohal, B Maity, S Basu, RSC Adv., (2021) 11, 25586

[57] Z Guo, B Cai, Q Cao, Y Su, M Li, J Hu, Z Yang, Y Zhang, Fullerenes Nanotubes Carbon Nanostruct (2017) 25 704–9.

[58] D Huang, H Zhou, Y Wu, T Wang, L Sun, P Gao, Y Sun, H Huang, G Zhou, J Hu, Carbon. (2019) 142:673–84.

[59] J Ou, Y Tao, J Xue, Y Kong, J Dai, L Deng,ElectrochemCommun. (2015) 57 5–9.

[60] F Hasanpour, M Nekoeinia, A Semnani, S Shojaei,Microchem J. (2018) 142 17–23.

[61] B Ramezanzadeh, B Karimi, M Ramezanzadeh, M Rostami,J Taiwan InstChem Eng. (2019) 95369–82.

[62] Y Luo, Y Wang, H Yan, Y Wu, C Zhu, D Du, Y Lin, Anal ChimActa. (2018) 104244–51.

[63] NR Ko, M Nafiujjaman, JS Lee, HN Lim, Yk Lee, IK Kwon, RSC Adv. (2017) 7 11420–7.

[64] B Liu, L Peng, W Chen, J Wang, T Han, Q Mo, NanosciNanotechnolLett. (2017) 9 297–300.

[65] R Liu, D Wu, X Feng, K Mullen, J Am ChemSoc. (2011) 133 15221–3.

[66] Y Luo, M Li, L Sun, Y Xu, M Li, G Hu, TTang, J Wen, X Li, J Zhang, L Wang, J Colloid Interface Sci. (2018) 529205–13.

[67] S Bian, C Shen, Y Qian, J Liu, F Xi, X Dong, Sens Actuators B Chem. (2017) 242 231–7.

[68] G Wang, Q Guo, D Chen, Z Liu, X Zheng, A Xu, S Yang, G Ding, ACS Appl MaterInterfaces. (2018) 105750–9.

[69] A Bayat, E Saievar-Iranizad, Energy Chem. (2018) 27306–10.

[70] TV Tam, WM Choi, CurrAppl Phys. (2018) 18 1255–60.

[71] Y Dong, J Shao, C Chen, H Li, R Wang, Y Chi, X Lin, G Chen, Carbon (2012) 12 4738-4743., J Gu, X Zhang, A Pang, J Yang, Nanotechnology (2016) 27 (16) 165704.

[72] X Hou, Y Li, C Zhao,Aust J Chem. 2016;69:357.

[73] AKAlves, ACS Frantz, FA Berutti,FlatChem. (2018) 12 26–34.

[74] B Fresco-Cala, ML Soriano, A Sciortino, M Cannas, F Messina, S Cardenas, RSC Adv.(2018) 8 29939–46.

[75] R Li, Y Liu, Z Li, J Shen, Y Yang, X Cui, G Yang, Chem. Eur. J. 1 (2016) 272-278.

[76] S Gao, L Tang, J Xiang, R Ji, SK Lai, S Yuan, SP Lau, New J. Chem. (2017) 18 10447-10451.

[77] J Lu, PSE Yeo, CK Gan, P Wu, KP Loh, Nat. Nanotechnol. (2011) 4 247-252.

[78] D Huang, L Yin, X Lu, S Lin, Z Niu, J Niu,ChemEng J. (2017) 323406–14.

[79] M Kaur, M Kaur, VK Sharma,AdvColl Interface Sci. (2018) 25944–64.

[80] Z Qin, JC Bischof, Chem. Soc. Rev. (2012) 41 1191−1217.

[81] CS Tshangana, AA Muleja, AT Kuvarega, TJMalefetse, BB Mamba, J. Water Process. Eng., (2021) 43 102249.

[82] SKundu, VK Pillai, Phys. Sci. Rev., (2020) 5 20190013

[83] V Vatanpour, S MousaviKhadem, M Masteri-Farahani,N Mosleh, M Ganjali, A Badiei, E Pourbashir,A Mashhadzadeh, MMunir, G Mahmodi, J. WaterProcess. Eng., (2020) 38 101652.

[84] M P Romero, F Alves, M D Stringasci, H H Buzzá, H Ciol, N M Inada,V S Bagnato, Front. Microbiol.(2021) 12 662149.

[85] J P Naik, P Sutradhar,MSaha, J NanostructChem (2017) 7:85–89.

[86]. J Peng, W Gao, B K Gupta, Z Liu,R Romero-Aburto, L Ge,L Song, L B Alemony, A A Marti, T Hayashi, J-J Zhu, P M Ajayan, Nano Lett. (2012) 12 844−849.

[87] NE Lee, SY Lee, HS Lim, SH Yoo, SO Cho, Nanomaterials,(2020) 10 277

[88] A Abbas, S Rubab, A Rehman, S Irfan, H M A Sharif, Q Liang, TA Tabish, Materials Today Chemistry (2023) 30 101555

[89] X Hai, Q-X Mao, W-J Wang, X-F Wang, X-W Chen, J-H Wang, J. Mater. Chem. B (2015) 3 9109-9114.

[90] Z Fan, Y Li, X Li, L Fan, S Zhou, D Fang, S Yang, Carbon (2014) 70 149-156.

[91] TV Tam, SG Kang, KF Babu, E-S Oh, SG Lee, WM Choi, J. Mater. Chem., A (2017) 5 10537-10543.

[92] F Qian, X Li, L Tang, SK Lai, C Lu, SP Lau, AIP Adv., (2016) 6 075116.

[93] N-U.Ain, MO Eriksson, S Schmidt, M Asghar, P-C Lin, PO Holtz,M Syväjärvi, GR Yazdi, Nanomaterials (Basel) (2016) 6 198.

[94] Q Li, S Zhang, L Dai, L-S Li, J. Am. Chem. Soc. (2012)134 18932-18935.

[95] P Tian, L Tang, K S Teng, S P Lau Materials today Chemistry (2018)10, 221

[96] H Li, C Sun, M Ali, F Zhou, X Zhang, DR MacFarlane, Angew. Chem. Int. Ed., (2015)54, 8420

[97] S Chinnusamy, R Kaur, A Bokare, F Erogbogbo MRSCommun., (2018) 8, 137

[98] D Chao, C Zhu, X Xia, J Liu, X Zhang, J Wang, P Liang, J Lin, H Zhang, ZX Shen, H.J. Fan Nano Lett., (2015)15, 565

[99] S Bose, T Kuila, T X H Nguyen, N H Kim, K-T Lau, J H Lee 86 J Peng, W Gao, B K Gupta, Z Liu,R Romero-Aburto, L Ge,L Song, LB Aleman, XZha,Gao,SAVithayathil, B A Kaipparettu, AA Marti, T Hayashi, J-J Zhu, PM Ajayan, Nano Lett. (2012) 12 844−849.

Wind turbine: Various types and its components

Subhendu Chandra

Department of Physics, Victoria Institution (College), 78-B, A. P. C. Road, Kolkata-700009

1. Abstract:

A wind turbine, or a wind energy converter, is a device that converts the wind's kinetic energy into electrical energy. Wind turbines are manufactured in a wide range of vertical and horizontal axis. The smallest turbines are used for applications such as battery charging for auxiliary power for boats or caravans or to power traffic warning signs. Larger turbines can be used for making contributions to a domestic power supply while selling unused power back to the utility supplier via the electrical grid. Arrays of large turbines are becoming an increasingly significant source of recurrent renewable energy and are used by many countries to reduce their reliance on fossil fuels.

2. Introduction:

Wind turbine is a machine which converts the power available in the wind into electricity [1, 2]. On the other hand, a windmill is a machine which was used to convert wind power to mechanical power. As generators of electricity, wind turbines are usually connected into some form of electrical network and the larger turbines can form a part of the electrical grid [3].

There has been a remarkable growth over the past four decades in global installed generating capacity. The data given from statistics published by the Global Wind Energy Council (GWEC), the European Wind Energy Association (EWEA), the American Wind Energy Association (AWEA), and others shows the regional and worldwide growth of installed wind power capacity up to the end of 2013 [4]. It is interesting to note that the global wind power capacity is now still doubling every 3 years. The biggest regional contributors to this installed growth in wind power are the People’s Republic of China. According to the GWEC, the development of wind energy in China in terms of scale is absolutely unparalleled in the world. By the end of 2010, the installed wind power capacity had reached 41.8 GW. Up to May 2009, 80 countries around the world

contributed to the generation of wind power on a commercial scale. Predicting the growth of wind power generation is far from reliable [5].

3. Various Types of Turbines

Wind turbines can rotate about either a horizontal or a vertical axis, the former being both older and more common. They can also include blades, or be blade less. Vertical designs produce less power and are less common [6].

3.1 Horizontal axis

Large three-bladed horizontal-axis wind turbines (HAWT) [7] with the blades upwind of the tower produce the overwhelming majority of wind power in the world today. These turbines have the main rotor shaft and electrical generator at the top of a tower, and must be pointed into the wind. Small turbines are pointed by a simple wind vane, while large turbines generally use a wind sensor coupled with a yaw system. Most have a gearbox, which turns the slow rotation of the blades into a quicker rotation that is more suitable to drive an electrical generator. Some turbines use a different type of generator suited to slower rotational speed input. These don't need a gearbox and are called direct-drive, meaning they couple the rotor directly to the generator with no gearbox in between. While permanent magnet direct-drive generators can be more costly due to the rare earth materials required, these gearless turbines are sometimes preferred over gearbox generators because they "eliminate the gear-speed increaser, which is susceptible to significant accumulated fatigue torque loading, related reliability issues, and maintenance costs. There is also the pseudo direct drive mechanism, which has some advantages over the permanent magnet direct drive mechanism.

Most horizontal axis turbines have their rotors upwind of the supporting tower. Downwind machines have been built, because they don't need an additional mechanism for keeping them in line with the wind. In high winds, the blades can also be allowed to bend, which reduces their swept area and thus their wind resistance. Despite these advantages, upwind designs are preferred, because the change in loading from the wind as each blade passes behind the supporting tower can cause damage to the turbine.

Turbines used in wind farms for commercial production of electric power are usually three-bladed. These have low torque ripple, which contributes to good reliability.

The blades are usually coloured white for daytime visibility by aircraft and range in length from 20 to 80 meters. The size and height of turbines increase year by year. Offshore wind turbines are built up to 8 MW today and have a blade length up to 80 meters. Usual multi megawatt turbines have tubular steel towers with a height of 70 m to 120 m and in extremes up to 160 m.

3.2 Vertical axis

Vertical-axis wind turbines (or VAWTs) have the main rotor shaft arranged vertically. One advantage of this arrangement is that the turbine does not need to be pointed into the wind to be effective, which is an advantage on a site where the wind direction is highly variable. It is also an advantage when the turbine is integrated into a building because it is inherently less steerable. Also, the generator and gearbox can be placed near the ground, using a direct drive from the rotor assembly to the ground-based gearbox, improving accessibility for maintenance. However, these designs produce much less energy averaged over time, which is a major drawback [8].

The key disadvantages include the relatively low rotational speed with the consequential higher torque and hence higher cost of the drive train, the inherently lower power coefficient, the 360-degree rotation of the aerofoil within the wind flow during each cycle and hence the highly dynamic loading on the blade, the pulsating torque generated by some rotor designs on the drive train, and the difficulty of modelling the wind flow accurately and hence the challenges of analysing and designing the rotor prior to fabricating a prototype.

When a turbine is mounted on a rooftop the building generally redirects wind over the roof and this can double the wind speed at the turbine. If the height of a rooftop mounted turbine tower is approximately 50% of the building height it is near the optimum for maximum wind energy and minimum wind turbulence.

Sub-types of the vertical axis design include:

3.2.1 Darrieus wind turbine

"Eggbeater" turbines, or Darrieus turbines [9], were named after the French inventor, Georges Darrieus. They have good efficiency, but produce large torque ripple and

cyclical stress on the tower, which contributes to poor reliability. They also generally require some external power source, or an additional Savonius rotor to start turning, because the starting torque is very low. The torque ripple is reduced by using three or more blades, which results in greater solidity of the rotor. Solidity is measured by blade area divided by the rotor area. Newer Darrieus type turbines are not held up by guy-wires but have an external superstructure connected to the top bearing.

3.2.2 Giromill

A sub-type of Darrieus turbine with straight, as opposed to curved, blades. The cycloturbine variety has variable pitch to reduce the torque pulsation and is self-starting. The advantages of variable pitch are: high starting torque; a wide, relatively flat torque curve; a higher coefficient of performance; more efficient operation in turbulent winds; and a lower blade speed ratio which lowers blade bending stresses. Straight, V, or curved blades may be used [10].

3.2.3 Savonius wind turbine

These are drag-type devices with two (or more) scoops that are used in anemometers, Flettner vents (commonly seen on bus and van roofs), and in some high-reliability low-efficiency power turbines. They are always self-starting if there are at least three scoops. Twisted Savonius is a modified savonius, with long helical scoops to provide smooth torque. This is often used as a rooftop wind turbine and has even been adapted for ships [11].

3.2.4 Parallel

The parallel turbine [12] is similar to the cross flow fan or centrifugal fan. It uses the ground effect. Vertical axis turbines of this type have been tried for many years: a unit producing 10 kW was built by Israeli wind pioneer Bruce Brill in the 1980s.

4. Various components of Wind Turbines

Figure 1 represent the details structure of the turbine and its various components [13]

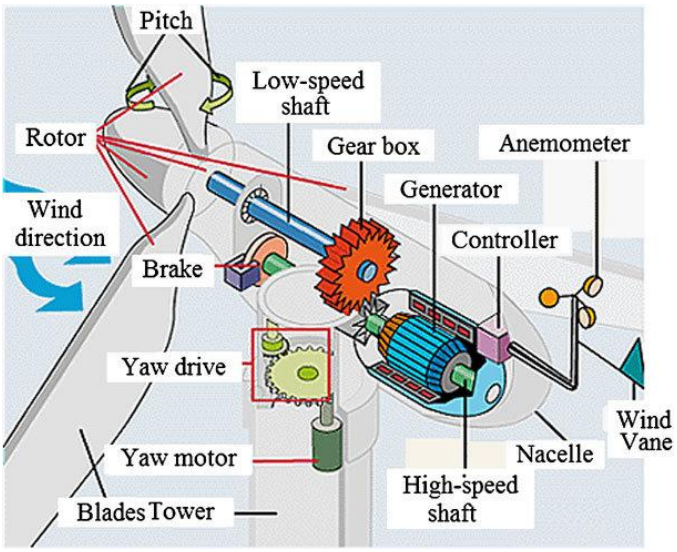

Figure 1

4.1 Anemometer: Measures the wind speed and transmits wind speed data to the controller.

4.2 Blades: Lifts and rotates when wind is blown over them, causing the rotor to spin. Most turbines have either two or three blades.

4.3 Brake: Stops the rotor mechanically, electrically, or hydraulically, in emergencies.

4.4 Controller: Starts up the machine at wind speeds of about 8 to 16 miles per hour (mph) and shuts off the machine at about 55 mph. Turbines do not operate at wind speeds above about 55 mph because they may be damaged by the high winds.

4.5 Gear box: Connects the low-speed shaft to the high-speed shaft and increases the rotational speeds from about 30-60 rotations per minute (rpm), to about 1,000-1,800 rpm; this is the rotational speed required by most generators to produce electricity. The gear box is a costly (and heavy) part of the wind turbine and engineers are exploring "direct-drive" generators that operate at lower rotational speeds and don't need gear boxes.

4.6 Generator: Produces 50-cycle AC electricity; it is usually an off-the-shelf induction generator.

4.7 High-speed shaft: Drives the generator.

4.8 Low-speed shaft: Turns the low-speed shaft at about 30-60 rpm.

4.9 Nacelle: Sits atop the tower and contains the gear box, low- and high-speed shafts, generator, controller, and brake. Some nacelles are large enough for a helicopter to land on.

4.10 Pitch: Turns (or pitches) blades out of the wind to control the rotor speed, and to keep the rotor from turning in winds that are too high or too low to produce electricity.

4.11 Rotor: Blades and hub together form the rotor.

4.12 Tower: Made from tubular steel (shown here), concrete, or steel lattice. Supports the structure of the turbine. Because wind speed increases with height, taller towers enable turbines to capture more energy and generate more electricity.

4.13 Wind direction: Determines the design of the turbine. Upwind turbines—like the one shown here—face into the wind while downwind turbines face away.

4.14 Wind vane: Measures wind direction and communicates with the yaw drive to orient the turbine properly with respect to the wind.

4.15 Yaw drive: Orients upwind turbines to keep them facing the wind when the direction changes. Downwind turbines don't require a yaw drive because the wind manually blows the rotor away from it.

4.16 Yaw motor: Powers the yaw drive.

5. Power Calculation of the Wind Turbine

The following table shows the definition of various variables used in this model [14]:

$$E = Kinetic\ Energy\ (J), \rho = Density\ \left(\frac{Kg}{m^3}\right), m = mass\ (Kg), A = Swept\ Area\ (m^2\ ),$$

$$v = Wnnd\ Speed\ \left(\frac{m}{s}\right), c_p = power\ Coefficient, p = Power\ (Watt), r = Radius\ (m),$$

$$\frac{dm}{dt} = Mass\ flow\ rate\ \left(\frac{Kg}{s}\right), x = distance\ (m), \frac{dE}{dt} = Energy\ flow\ Rate\ \left(\frac{J}{s}\right), t = Time\ (s)$$

Under constant acceleration, the kinetic energy of an object having mass *m* and velocity *v* is equal to the work done *W* in displacing that object from rest to a distance *s* under a force *F*, i.e.:

$$E = W = FS$$

According to Newton's Law, we have:

$$F = ma$$

Hence,

$$E = mas \qquad (1)$$

Using the third equation of motion:

$$v^2 = u^2 + 2as$$

we get:

$$a = \frac{v^2 - u^2}{2s}$$

Since the initial velocity of the object is zero, i.e. $u = 0$, we get:

$$a = \frac{v^2}{2s}$$

Substituting it in equation (1), we get that the kinetic energy of a mass in motions is:

$$E = \frac{1}{2}mv^2 \qquad (2)$$

The power in the wind is given by the rate of change of energy:

$$P = \frac{dE}{dt} = \frac{1}{2}v^2\frac{dm}{dt} \qquad (3)$$

As mass flow rate is given by:

$$\frac{dm}{dt} = \rho A\frac{dx}{dt}$$

and the rate of change of distance is given by:

$$\frac{dm}{dt} = \rho Av$$

Hence, from equation (3), the power can be defined as:

$$P = \frac{1}{2}\rho Av^3 \qquad (4)$$

6. Conclusions:

The development of non-conventional energy sources are very essential for the society of the developing country like us through proper scientific motivation and technological advancement. Wind energy is one of the most powerful non-conventional energy source among all the natural energy sources throughout the world. Various types of turbines and its different components along with working principles explain here elaborately. Through power calculation of the turbine one can control the use of available power and can optimize the ratio of power consumed over the power generation.

References:

[1] 5.17 Energy Management in Wind Energy Systems, Eftichios Koutroulis, Comprehensive Energy Systems, Volume 5, 2018, Pages 707-741

[2] Chapter 15 - Doubly Fed Induction Generator in Wind Energy Conversion Systems, Domingos S.L. Simonetti, Arthur E.A. Amorim, Flávio D.C. Oliveira, Advances in Renewable Energies and Power Technologies, Volume 1: Solar and Wind Energies, 2018, Pages 461-490

[3] High-resolution large-scale onshore wind energy assessments: A review of potential definitions, methodologies and future research needs, Russell McKenna, Stefan Pfenninger, Heidi Heinrichs, Johannes Schmidt, Iain Staffell, Christian Bauer, Katharina Gruber, Andrea N. Hahmann, Malte Jansen, Michael Klingler, Natascha Landwehr, Xiaoli Guo Larsén, Johan Lilliestam, Bryn Pickering, Martin Robinius, Tim Tröndle, Olga Turkovska, Sebastian Wehrle, Jann Michael Weinand, Jan Wohland, Renewable Energy, Volume 182, January 2022, Pages 659-684

[4] GLOBAL WIND REPORT ANNUAL MARKET UPDATE 2013, Steve Sawyer, Secretary General, Global Wind Energy Council, Klaus Rave, Chairman, Global Wind Energy Council

[5] About Wind Energy / Why Wind Energy, Installed Wind Power Capacity, Update: to see 2011 rankings, check out: https://cleantechnica.com/world-wind-power/2/

[6] Introduction to wind energy systems, The European Physical Journal Conferences Published by EDP Sciences, H.-J. Wagner, DOI: 10.1051/epjconf/20135401011

[7] DESIGN HORIZONTAL AXIS WIND TURBINE WITH THREE BLADES, Basuki Winarno, Imam Basuki, Ali Safi' I, JEEMECS Vol. 1, No. 1, FEBRUARY 2018, Online ISSN: 2100-014X

[8] A Review On The Types Of Vertical Axis Wind Turbines And The Methods Of Their Performance Study, Abdullah M A El-Zafry, Cairo, Esaim Mustafa Abrahim Omar, Esaim Mustafa Abrahim Omar et al. Journal of Multidisciplinary Engineering Science and Technology (JMEST)ISSN: 2458-9403Vol. 6 Issue 9, 2019

[9] Efficiency-based design optimization of the H-type Darrieus wind turbine with fixed guiding-walls, Roaa Ansaf, H.S. Abdelhameed, Islam Hashem, Zambri Harun, Energy Reports, Volume 9, December 2023, Pages 3576-3592

[10] Analysis and Design of a Giromill Type Vertical AxisWind Turbine for a Low Wind Profile Urban Area, A.Mohanasundaram, Dr. P. Valsalal, Journal of Electrical Engineering, 2020

[11] An Experimental Study on the Performance of Savonius Wind Turbines Related With The Number Of Blades, Frederikus Wenehenubuna, Andy Saputraa, Hadi Sutanto, Energy Procedia 68 (2015) 297 – 304

[12] A Study on the Parallel Operation Strategy of Small Wind Turbine System for Battery Charging, Yung-Deug Son, Hyun-Keun Ku, Jang-Mok Kim, The Transactions of the Korean Institute of Power Electronics Published by The Korean Institute of Power Electrics Print ISSN: 1229-2214, 19(6):549-556, DOI: 10.6113/TKPE.2014.19.6.549

[13] Clean and Sustainable Energy Technologies, M. Arshad, in Clean Energy for Sustainable Development, 2017

[14] Theoretical calculation of the power of wind turbine or tidal turbine, Pierre Lecanu Pierre, Lecanu Joël Bréard, Dominique Mouazé, Content uploaded by Pierre Lecanu, June 19, 2023

INFORMATION TO AUTHORS

Manuscripts should represent results of original works on theoretical physics or experimental physics with theoretical background or on applied mathematics and topics of interdisciplinary nature. Letters to the Editor and Review articles in emerging areas are also published. Submission of the manuscript will be deemed to imply that it has not been published previously and is not under consideration for publication elsewhere (either partly or wholly) and further that, if accepted, it will not be published elsewhere. It is the right of the Editorial Board to accept or to reject the paper after taking into consideration the opinions of the referees.

Manuscripts may be submitted in pdf/MS word format to **admin@citphy.org or susilvcsarkar@gmail.com** Online submission of the paper through our **website: www.citphy.org** is also accepted. The file should be prepared with 1 cm margin on all sides and a line spacing of 1.5. The word format should be Times New Roman front type having front size 12.

The title of the paper should be short and self-explanatory. All the papers must have an abstract of not more than 200 words, the abstract page must not be a part of the main file. Abstract should be self-contained. It should be clear, concise and informative giving the scope of the research and significant results reported in the paper. Below the abstract four to six key words must be provided for indexing and information retrieval.

The main file should be divided into sections (and sub-sections, if necessary) starting preferably with introduction and ending with conclusion. Displayed formula must be clearly typed (with symbols defined) each on a separate line and well-separated from the adjacent text. Equations should be numbered with on the right-hand side consecutively throughout the text. Figures and Tables with captions should be numbered in Arabic numerals in the order of occurrence in the text and these should be embedded at appropriate places in the text. Associated symbols must invariably follow SI practice.

References should be cited in the text by the Arabic numerals as superscript. All the references to the published papers should be numbered serially by Arabic numerals and given at the end of the paper. Each reference should include the author's name, title, and abbreviated name of the journal, volume number, year of publication, and page numbers as in the simple citation given below:

For Periodicals : Sen, N. R. - On decay of energy spectrum of Isotopic Turbulence, 1. Appl. Phys. **28,** No. 10, 109-110 (1999).

1. Mikhilin, S. G. - Integral Equations, Pergamon Press, New York (1964).
2. Hinze, A. K. - Turbulence Study of Distributed Turbulent Boundary Layer Flow, Ph. D, Thesis, Rorke University (1970).

The corresponding author will receive page proof, typically as a pdf file. The proof should be checked carefully and returned to the editorial office within two or three days. Corrections to the proof should be restricted to printing errors and made according to standard practice. At this stage any modifications (if any) made in the text should be highlighted.

To support the cost of publication of the journal, the authors (or their Institutions) are requested to pay publication charge ` 200/- per printed page for authors of Indian Institutes and US$ 20 for others. Publication charges to be sent directly to **CALCUTTA INSTITUTE OF THEORETICAL PHYSICS, 'BIGNAN KUTIR', 4/1 MOHAN BAGAN LANE, KOLKATA-700004, INDIA.**

A pdf of the final publisher's version of the paper will be sent to the corresponding author.

All communications are to be sent to the Secretary, Calcutta Institute of Theoretical Physics, 'BignanKutir', 4/1, Mohan Bagan Lane, Kolkata-700004, India. E-mail:susilvcsarkar@gmail.com

For details please visit our website www.citphy.org

INDIAN JOURNAL OF THEORETICAL PHYSICS

BOARD OF EDITORS